Controlling Indoor Humidity Using Variable-Speed Compressors and Blowers

M. A. Andrade and C. W. Bullard

ACRC TR-151

July 1999

The Air Conditioning and Refrigeration Center was founded in 1988 with a grant from the estate of Richard W. Kritzer, the founder of Peerless of America Inc. A State of Illinois Technology Challenge Grant helped build the laboratory facilities. The ACRC receives continuing support from the Richard W. Kritzer Endowment and the National Science Foundation. The following organizations have also become sponsors of the Center.

Amana Refrigeration, Inc.
Brazeway, Inc.
Carrier Corporation
Caterpillar, Inc.
Chrysler Corporation
Copeland Corporation
Delphi Harrison Thermal Systems
Frigidaire Company
General Electric Company
Hill PHOENIX
Honeywell, Inc.
Hussmann Corporation
Hydro Aluminum Adrian, Inc.
Indiana Tube Corporation
Lennox International, Inc.
Modine Manufacturing Co.
Peerless of America, Inc.
The Trane Company
Thermo King Corporation
Visteon Automotive Systems
Whirlpool Corporation
York International, Inc.

For additional information:

Air Conditioning & Refrigeration Center
Mechanical & Industrial Engineering Dept.
University of Illinois
1206 West Green Street
Urbana IL 61801

217 333 3115

Abstract

Residential-scale a/c systems control indoor temperature but not humidity. The advent of variable-speed compressors and blowers make such control possible. This paper uses a detailed simulation model to explore the tradeoff between energy efficiency and comfort, as measured by indoor humidity. Simultaneous solution of heat and mass transfer equations for the building, along with simulation of the air conditioner, makes it possible to calculate indoor humidity as a function of outdoor dew point and infiltration rate.

The results presented in Chapter 4 show how indoor humidity can be lowered by decreasing the evaporator air flow rate, because the fin temperatures are reduced and remove more condensate. In a moderate climate condition (75°F indoor temperature, 80°F outdoor temperature and 70°F outdoor dew-point temperature), indoor relative humidity can be reduced from 61 to 57% by reducing the blower speed from 500 cfm/ton to 200 cfm/ton. In addition to the extra comfort, system power input, averaged over the on/off cycles, decreases for most climate conditions with this blower speed reduction. In a moderate climate (75/80/70), average power drops from 0.83 to 0.77 kW, a 7% decrease in power usage in addition to the increase in comfort.

Reducing the compressor speed, and therefore refrigerant mass flow rate, increases EER by utilizing the heat exchangers for longer runtimes at lower ΔT's. However the refrigerant-side ΔT becomes a larger fraction of the total ΔT, so the effect of reducing blower speed is diluted. Overall, the system runs more efficiently but for a longer time, removing the same sensible load and latent load, and preventing short-cycling that would increase indoor humidity. In the baseline climate (75/80/70) halving the compressor speed and reducing the blower speed from 500 to 200 cfm/ton has a negligible effect in indoor humidity, and reduces average power 33% from 0.83 to 0.56 kW.

Table of Contents

List of Tables

List of Figures

Chapter 1

Introduction

1.1 The importance of indoor humidity control

Indoor air quality (IAQ) experts are now recognizing the harmful effects of high indoor relative humidity not only to buildings and houses but also, and more important, to occupants. In response to these findings, ASHRAE has increased outside air requirements in buildings (ANSI/ASHRAE, 1989). The combination of increased ventilation requirements and better indoor humidity control poses significant challenges to HVAC equipment manufacturers. A variety of outside air preconditioning equipment are being promoted to address this challenge in buildings (Kosar, Witte, Shirey and Hedrick, 1998). In houses with small split systems and window units, however, these challenges have to be met without the advantage of preconditioning. Chuah, Hung and Tseng (1998) stated that "for dehumidification control, airflow rate is of prime concern". This prompted a study of the effect of evaporator airflow in indoor humidity.

1.2 Humidity loads

Harriman, Plager and Kosar (1997) have shown that except for desert climates, yearly latent loads exceed sensible loads by at least 3:1 in positive ventilation or infiltration air to maintain a comfortable indoor condition of 75° F, 50% relative humidity. This demonstrates the importance of dehumidification for a comfortable indoor environment, and a new direction in the HVAC industry: "... the need for ventilation air has forced HVAC equipment (originally optimized for high efficiency in removing sensible heat loads) to remove high moisture loads."

1.3 Analytical framework

Under mild temperature and high humidity outdoor conditions, the occupant usually sets the thermostat down below 75° F to achieve a comfortable indoor humidity. This artificially increases the sensible load raising the SHR (sensible heat ratio) of the load to the SHR of the a/c system. This report considers a different approach to this problem: an a/c system with the capability to decrease its SHR to match the load SHR.

Decreasing the blower speed is one possible way of changing the system's SHR, but it generally results in a lower EER.

This report also proposes a different framework for comparing such options, based on overall energy consumption instead of EER. Energy consumption is equal to EER times the load. The traditional approach has a higher EER than the proposed solution, but it also has a higher load.

Finally in this report considers the potential for modulating compressor capacity at the same time as evaporator airflow. Analytically, we specify a target indoor comfort condition (temperature and relative humidity) and calculate the blower speed and compressor speed required to achieve it.

Chapter 2

Model Changes and Validation

Two major changes were made to the air conditioner simulation model. It was modified to handle split systems in addition to window a/c units. Changes were also made to the evaporator heat and mass transfer equations, implementing results of a validation study by Kirby, Bullard and Dunn (1998).

2.1 Window unit validation

Kirby, Bullard and Dunn (1998) presented measured data for a 1.5 ton Whirlpool room a/c system wet-coil conditions. Those results were compared with predicted values using a simple three zone evaporator model (Bridges and Bullard, 1995). This comparison showed that the model had excellent overall heat transfer predictions (300 Btu/hr bias error, and a 95% confidence interval of 300 Btu/hr, for a total error of 600 Btu/hr, or 3% of the nominal capacity of the evaporator). However, the water removal rate predictions did not correlate to the measured data as well as the overall heat transfer (total error of 1.5 lbm/hr, or 25% of the average water removal rate for the points in question.)

To verify that the error was not due to the large airflow non-uniformity present in room a/c units, an identical evaporator was tested in a wind tunnel under ideal conditions. The discrepancy in water removal predictions persisted. Therefore the mass transfer equations were re-examined and modified as described in Section 2.2 bellow.

2.2 Evaporator model changes

When operating under wet conditions, the heat transfer between air and the evaporator surface has two components, latent and sensible. The total heat transfer between the air and the evaporator has to be equal to the heat transfer between the evaporator and the refrigerant

When modeling dry cases, it does not matter whether the fin efficiency is viewed as increasing fin temperature or reducing fin area. Reducing fin area has the same effect as reducing the temperature difference between the fin and the air since both area and temperature difference are linearly proportional to sensible heat transfer. Physically, however, the driving potential for the latent heat transfer mode is the humidity difference

3

between the fin and air. Humidity difference is not linearly proportional to temperature difference, therefore for wet cases it does make a difference whether fin efficiency is used to reduce the area available for heat transfer, or to reduce the temperature difference between air and the fin. As pointed out by Kirby, Bullard and Dunn (1998), the fin surface efficiency should be used to calculate the extent to which the surface of the fin is warmer than the evaporator tube. This works like an extra heat transfer resistance between the tube and the fins.

$$(2) \qquad \eta_{surf} = \frac{T_{air} - T_{fin}}{T_{air} - T_{tube}}$$

For simplicity, their model assumed a Lewis number of 1. That assumption has since been eliminated, and now the model calculates the actual Lewis number and uses that to calculate the mass transfer coefficient.

Water removal predictions depend strongly on the evaporator fin temperature prediction, and further improvement in the condensate removal prediction would be possible by improving the fin temperature prediction. Earlier calculations used a simple arithmetic average humidity and temperature differences to calculate the water removal in the evaporator, which introduces error in the water removal prediction because the relationship is not exactly linear. To further reduce the error, the model now uses log mean differences.

The new version of the model was compared with the old version using data from Kirby, Bullard and Dunn (1998). The new version improved the water removal bias error significantly (0.34 lbm/hr for the new model versus 0.71 lbm/hr for the old model). The 95% confidence interval also improved (0.70 lbm/hr down from 0.84 lbm/hr with the old model), although not as dramatically as the bias error. Therefore the total error in the water removal prediction went from 1.55 lbm/hr in the old model to 1.04 lbm/hr in the new model. Figure 2.2.1 shows a plot of the old and the new predicted water removal versus the measured value. All the points fall within ±1 lbm/hr of the measured value.

4
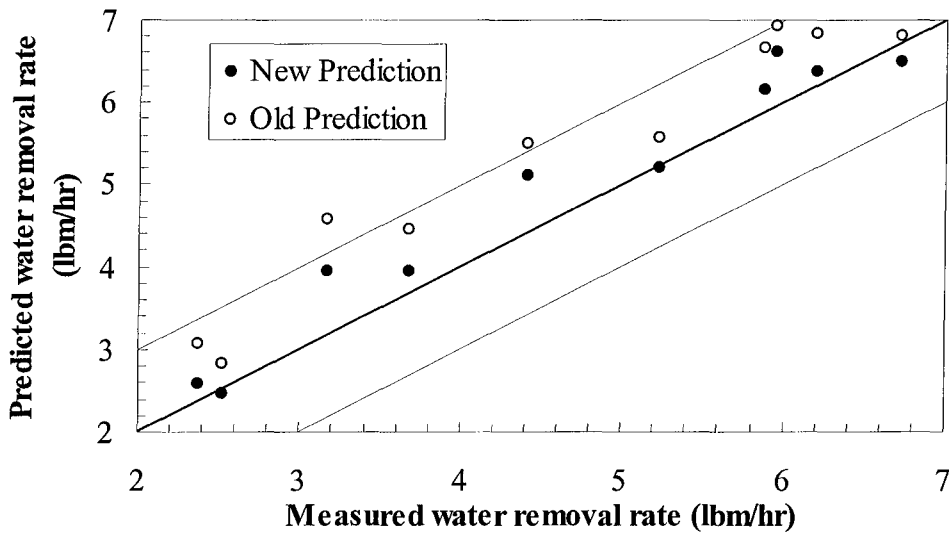
Figure 2.2.1: Water removal prediction in the Whirlpool window unit.

There are only a few possible explanations for the overprediction error shown in Figure 2.2.1; most assumptions would tend to cause underprediction (e.g. increased surface area and horseshoe vortices enhancing heat and mass transfer downstream of water droplets of latent heat transfer). One possibility is the insulating effect of the water droplets or film. Another possibility is that the kinetics of mass transfer proceed at an inherently slower rate than heat transfer, so equilibrium conditions are not achieved during the 33 milliseconds that air is passing over the fin.

2.3 Split system model changes

The simulation model was initially developed by Bridges and Bullard (1995) to simulate a/c window units. While the main components are the same in a split system, there are some physical differences between these two types of residential a/c units that make it necessary to modify the equations to simulate split systems.

Window units have only one motor that connects to both the evaporator blower and the condenser fan, while split systems have two separate motors, so the appropriate equations were added. Also, for split systems, the evaporator blower power (in watts) is calculated based on volumetric flow (cfm), according to the equation in the ARI standard:

(1) $Fan\ Power\ =\ \dot{V}_{air}\ \times 0.365$

5

For a 3-ton system, using a rule of thumb value of 400 cfm/ton, the evaporator blower would have a 1200 cfm/ton and use 438 watts of power (1200 cfm/ton times 0.365 watts/cfm/ton). According to the fan laws ASHRAE (1997), fan power varies with the cubic changes in volumetric flow. Therefore the evaporator blower power equation becomes:

$$(2) \qquad FanPower = (\dot{V}_{air} / 1200)^3 \times 438$$

Another major difference between window units and split systems is in the air routing. In window units, the outdoor air flows over the compressor first, then the condenser fan, and finally through the condenser. In many split systems, outdoor air flows by the condenser first, and then the compressor and finally the fan. This different air path is reflected in the heat transfer equations for the condenser, as well as the air temperature to which heat is rejected by both the condenser and compressor shell. The heat transfer in the discharge line is similarly affected.

2.4 Split system validation

A Carrier 3-ton split system using R-410A was also modeled and tested in the ACRC (Yin, 1998). Both the evaporator and the condenser have wavy fins enhanced with arrays of small offset strips. Therefore the model was modified to handle those geometries.

2.4.1 Enhanced fins

Nakayama and Xu (1983) proposed using a correction to plain fins to calculate the j-factor for this type of fin, and found that the most important geometrical parameters were fin spacing and the fraction of the area enhanced. Fin spacing is calculated using the ratio of fin thickness (δ_f) and gap width between neighboring fins (δ_a) calculated as:

$$(3) \qquad \delta_a = \frac{1}{p_f} - \delta_f$$

The ratio of enhanced to total fin area (ϕ_s) is calculated by

$$(4) \qquad \phi_s = \frac{(2n_s - 1)l_s s_s}{S_t S_l - \pi d_{eff}^2 / 4}$$

6

where n_s is the number of raised strips in an enhanced zone, l_s is the width of the strips, s_s is the length of the strips, S_t and S_l are the vertical and horizontal tube spacings, and d_{eff} is the effective tube diameter. For the Carrier fin, ϕ_s is equal to 0.336.

Nakayama and Xu (1983) suggest a j-factor correction (F_t) to account for this enhancement of the form

(5) $\qquad j = Plain\ fin\ correlation \times F_j$

(6) $\qquad F_j = 1 + 1.093 \times 10^3 \left(\dfrac{\delta_f}{\delta_a} \right)^{1.24} \phi_s^{0.944} Re^{-0.58} + 1.097 \left(\dfrac{\delta_f}{\delta_a} \right)^{2.09} \phi_s^{2.26} Re^{0.88}$

where the Reynolds number is based on the hydraulic diameter of the free-flow area. This enhancement factor is valid for:

- $250 \leq Re \leq 3000$
- 0.15 mm (0.0059 in) $\leq \delta_f \leq$ 0.2 mm (0.0079 in)
- 1.8 mm (169 fins/ft) $\leq p_f \leq$ 2.5 mm (122 fins/ft)
- $0.2 \leq \phi_s \leq 0.35$

Under normal operating conditions, the airflow through the evaporator in the 3-ton split system has a Reynolds number around 500, within the range of applicability for Nakayama and Xu's correction. The test unit has denser (174 fins/ft) and thinner (0.0045 in) fins than the heat exchangers used by Nakayama and Xu to obtain their correlation. However, the fin spacing parameter δ_f/δ_a for the evaporator fins (0.0698) falls between the minimum (0.0638) and maximum (0.125) values achievable within the acceptable ranges of fin thickness and fin pitch. Therefore Nakayama and Xu's correction factor was used for the fin pitch and fin thickness values for the evaporator.

2.4.2 Plain fin correlation

The Nakayama and Xu enhancement factor was designed to be applied to a plain fin correlation. Therefore, it is necessary to select a plain fin correlation to use with the model. There are several correlations for fin-and-tube heat exchangers in the literature. However, modern heat exchangers have smaller diameter tubes (9.5 mm or 0.375 in), and more closely packed fins (174 fins/ft) than the heat exchangers used to developed the older correlations.

For our case, the fin is too thin (0.0045 in) to use the Elmahdy and Biggs (1979) correlation that worked best for the Whirlpool window unit (Kirby, Bullard and Dunn,

1998) (minimum fin thickness of 0.006 in). Wang and Chang (1998) point out that "The Gray and Webb correlation considerably under-predicts the present 7.0 and 9.5 mm tube diameter plain fin samples." Therefore, a newer correlation is needed to accurately predict heat transfer in the Carrier split system.

Wang and Chang (1998) propose a modified version of the Gray and Webb (1986) correlation of the form:

$$(7) \qquad j_4 = 0.357 \, Re_{Dc}^{-0.328} \left(\frac{P_t}{P_l} \right)^{-0.502} \left(\frac{s}{D_c} \right)^{0.0312} \left(\frac{P_t}{D_c} \right)^{-1.28}$$

$$(8) \qquad \frac{j_N}{j_4} = 0.991 \left[2.24 \, Re_{Dc}^{-0.092} \left(\frac{N}{4} \right)^{-0.031} \right]^{0.607(4-N)}$$

where j_4 is the j-factor for a heat exchanger with 4 or more rows, and j_N is the j-factor for a heat exchanger with N tube rows (3 or less). P_t is the transverse tube pitch, P_l is the longitudinal tube pitch, s is fin spacing, D_c is the tube outside diameter (including collar thickness), and Re_{Dc} is the Reynolds number based on that diameter.

This correlation was derived using newer heat exchangers, and therefore should work better than the older correlations. Table 2.4.1 shows that indeed the Wang and Chang correlation works best in simulating the 3-ton system under ARI Standard A conditions (Carrier, 1997). Therefore the Wang and Chang correlation will be used in all computer simulation in this report.

	Test data	Wang and Chang	Error (%)	Elmahdy and Biggs	Error (%)	Gray and Webb	Error (%)
Net capacity (kBtu/hr)	35	34.1	-2.44	35.3	0.80	36.6	4.48
Net sensible (kBtu/hr)	25.3	24.5	-3.25	30.5	20.71	25.6	1.20
Latent capacity (kBtu/hr)	9.7	9.7	0.33	4.7	-51.16	11.0	13.01
SHR	0.723	0.717	-0.83	0.866	19.76	0.700	-3.13

Table 2.4.1: Heat transfer correlation comparison for ARI Standard A point.

2.5 Variable speed compressor

A very crude model is used to simulate compressor mass flow modulation. A modulating factor (Beta) multiplies both the compressor mass flow rate and power found from the full-speed compressor map.

Chapter 3

Indoor humidity issues

3.1 Comfort considerations

The main reason people use air conditioning units is for comfort. They want the a/c unit to keep the room at a temperature that feels good, not too warm or too cold. That is easily achieved by having a unit that matches the heat load of the room in an extremely hot day, and cycles in more moderate days to keep the room in that comfortable temperature range. However, there is another component to human beings' comfort, humidity. People do not want to be in an environment (in this case a room) that feels too dry or too humid. Air conditioning units should therefore be able to control the humidity in a room to keep it in that comfort zone where the air is not too dry or too damp. Typically a/c units try to maintain 75 F and 50% relative humidity indoors, which most people find quite comfortable. Since 80 F is the ARI standard test condition, it will be used in the following analysis.

When air with constant absolute humidity is cooled, the relative humidity goes up. Since people's perception of humidity is relative humidity, a cool room would feel damper than a warm room even though they have the same absolute humidity. Air conditioning units cool the room, so they usually have to remove water from the room to keep the humidity in the comfort zone. Indoor air flows past the evaporator coils, where it cools down to the point where the water retained in the air condenses on the coil, drips down to the bottom of the a/c unit, and then flows to the outside. So there are basically two ways to control the humidity in the indoor room, change the amount of air that goes past the coil, or change the evaporator surface temperature, such that more or less water condenses on the evaporator coils.

3.2 Typical loads

Heat is added to a room in two forms, sensible and latent. Sensible heat is added to the room by heat transfer through the walls and the ceiling, warm air infiltrating into the room, body heat, appliances, etc. Latent heat load consists of humid air infiltration,

people breathing, humidity stored in wood, paper and clothes that is liberated to the room, people taking showers, cooking, etc.

Sensible and latent loads for a 20,000 ft^3 house (50' x 40' x 10') were estimated under different outside conditions. An infiltration rate of 1 air change per hour, and an R value of 10 for the walls and ceiling were assumed to calculate the external loads. The ceiling loads are overestimated because R-30 is more typical, but radiative loads through windows are underestimated by this simple calculation. It was also assumed that 4 people were in the house doing the equivalent of light office work, and appliances adding up to 200 watts to calculate the internal loads in the house. The ratio of the sensible to the total heat transfer load to the house is presented in bellow in Table 3.2.1 for several outdoor conditions.

T_{out} \ T_{dp}	62	65	70	75
82	0.63 (0.17)	0.44 (0.24)	0.29 (0.37)	0,20 (0.52)
85	0.74 (0.24)	0,58 (0.31)	0.40 (0.44)	0.30 (0.59)
90	0.83 (0.36)	0.70 (0.43)	0.53 (0.56)	0.42 (0.72)
95	0.87 (0.49)	0.76 (0.55)	0.62 (0.69)	0.50 (0.84)
100	0.90 (0.61)	0.81 (0,68)	0.67 (0.81)	0.57 (0.96)
105	0.91 (0.73)	0.84 (0.80)	0.72 (0.93)	xxx
110	0.93 (0.85)	0.86 (0.92)	xxx	xxx
115	0.94 (0.97)	xxx	Xxx	xxx

Table 3.2.1: SHR and (runtime fraction) for an a/c under several conditions

Table 3.2.1 shows the relative importance of latent loads increase at lower outdoor temperatures (low SHR). If the outdoor conditions are such that the outdoor temperature is close to the design indoor temperature, but the outdoor humidity is much higher than the design indoor humidity, the sensible load to the system would be reduced to radiation, and internal generation. Therefore the total load would be only a fraction of the design load, and the sensible heat ratio (SHR) of the system would be much lower than the usual system performance (0.75 for split systems, and 0.65 for window units at

the standard ARI capacity rating condition). To magnify the problem, a/c units short-cycle under low sensible loads which prevents the evaporator surface to condense enough water so that moisture removal starts.

These figures are only approximate, because they are based on the arbitrary assumption that indoor relative humidity is somehow held constant at 50%. In practice, the actual humidity level is a function of the house and the performance characteristics of both the house and the a/c unit. It results from a balance between loads and capacities, as described below.

3.3 House modeling

A simple house model was added to the program to calculate indoor humidity at various outdoor conditions, and to examine strategies for controlling it by varying blower and compressor speed. This addition consists of 8 new equations added to the model.

These sensible cooling load (LoadSen) of the house is calculated as

$$Load_{Sen} = (UA_{house} + m_{a,inf} * C_{p,wet}) * (T_{outdoor} - T_{indoor}) + 230 * Num_{People} + 3200$$

The first two terms account for the external load and the infiltration to the house, where UA_{house} is the overall UA of the house including both convection and radiation effects, $m_{a,inf}$ is the mass of air infiltrating the house, $C_{p,wet}$ is the specific heat of the moist air, $T_{outdoor}$ and T_{indoor} are the outdoor and indoor temperatures respectively. The third term accounts for body heat inside the house, where 230 Btu/hr is the body heat of person with low level of activity (watching TV or reading), and Num_{People} is the number of people inside the house. The last term accounts for the heat coming from appliances and lighting.

The latent cooling load (LoadLat) has only an infiltration term. Respiration and humidity produced inside the house (from cooking and showers) were neglected. Therefore, the latent load is written as

$$Load_{Lat} = (m_{a,inf} * h_{fg} * (w_{outdoor} - w_{air,E,i}))$$

where $w_{outdoor}$ and $w_{air,E,i}$ are the outdoor and indoor absolute humidities respectively.

The total load (Load) is the sum of the sensible and latent loads, the load sensible heat ratio (SHR_{Load}) is equal to the sensible load divided by the total load.

The mass of air infiltrating the house is calculated as

$$m_{a,inf} = V_{house} * ACH / v_a$$

where V_{house} is the volume of the house, ACH is number of air changes per hour, and v_a is the specific volume of air at the outdoor temperature.

The number of air changes per hour is calculated as a function of outdoor temperature (based on a table in the ASHRAE Fundamentals). It assumes 7.5 mph winds (summer average), and an indoor temperature of 75°F. Three different equations are found for a tightly, medium, and loosely sealed house.

Tightly sealed house: $ACH = 0.16 + T_{outdoor} * 0.002$

Loosely sealed house use: $ACH = 0.34 + T_{outdoor} * 0.004$

Medium sealed house use: $ACH = 0.12 + T_{outdoor} * 0.004$

Temperature control in an a/c system is basically a thermostat that turns the compressor on and off to try to keep a constant temperature. To simulate this, we calculate the fraction of time the unit would be on to maintain the specified indoor temperature (OnTime) as the total cooling load divided by the a/c unit's total cooling capacity.

OnTime = (Load/qEvap)

To simulate an equilibrium indoor humidity, we set the unit's sensible heat ratio equal to the cooling load sensible heat ratio. Since the total capacity is equal to the total load due to compressor cycling, equal sensible heat ratios mean that the unit removes as much humidity from the house as it comes in.

$SHR = SHR_{Load}$

If the user defines the outdoor conditions (temperature and humidity) and indoor temperature, and the house parameters (volume, UA, and the number of people inside), the model will solve for the fraction of time the compressor is on and the equilibrium indoor humidity. Results are shown in Chapter 4. Since these equations were added to the model in the same Newton-Raphson framework as the rest of the model, the user can swap variables and parameters. Among other combinations, the user can swap OnTime with Tindoor, and solve for an equilibrium indoor temperature and humidity; or swap indoor humidity and outdoor humidity to turn the house equations off (the model solves for an "equilibrium outdoor humidity" and OnTime fraction that the user can ignore).

Chapter 4

Using blower and compressor speed to control indoor humidity

A quick look at the Carnot refrigeration shows that one way to increase the efficiency of an air conditioner is to increase the evaporator temperature. However, as it will be shown, raising the evaporator temperature would decrease the water removal capability of the air conditioner and indoors ambient in humid areas would feel too damp. Since the HVAC industry has to design units that provide adequate cooling to vastly different environments, they chose to sacrifice efficiency for a better water removal rate to satisfy customers in humid areas. One way to go around this is to maximize the evaporator temperature (and therefore the a/c efficiency) under normal conditions, and use a mechanism to decrease the evaporator temperature under humid conditions to provide the extra water removal needed.

4.1 Humidity control

To keep a room comfortable, an a/c unit must control the indoor temperature, and humidity. In some large office buildings, a chiller cools the air below the delivered air state such that the air is saturated (100% relative humidity), and with the desired absolute humidity. Then a heater warms the air up to the delivered state, if it is still too cold after mixing in the duct with recirculated air.

Basically the chiller dehumidifies the air, at the cost of cooling the air too much, and the heater controls the air temperature. The chiller matches the latent load, and exceeds the total cooling needed. Then the total cooling is adjusted by adding sensible heat to the air, either from a heater or from an economizer that extracted heat from exhaust air.

In room a/c, the unit matches the sensible cooling load (via on-time fraction), and the latent load is whatever comes out. There is no separate control for the indoor humidity. The a/c unit has a fixed capacity and SHR for a given specific condition (indoor and outdoor temperatures and humidities). The on-time fraction matches the sensible cooling capacity with the room load, but there is no adjustment between the latent cooling and the latent load. The evaporator is designed such that the SHR is around 0.65 for window units, and 0.75 for split systems under the wet rating condition.

These numbers are rules of thumb developed by the a/c industry based on past experience, and ensure a comfortable indoor environment under most conditions.

Krakow, Lin and Zeng (1995) showed the suitability of controlling indoor temperature using a variable speed compressor, and indoor humidity using a variable speed evaporator blower.

4.2 Sensible heat ratio

Air conditioners remove heat from a room in two forms, sensible heat (cooling the air in the room), and latent heat (heat removed by condensing water on the evaporator coils). The ratio of sensible heat to total heat removed from a room is called the sensible heat ratio (SHR). At steady state, the total sensible and latent heat removed from the room must equal the total sensible and latent heat added to the room.

Both the sensible and latent heat load can be considered quasi-steady since they change very slowly. Therefore, if a room is to maintain steady-state temperature and humidity, the a/c unit must match the room's total load and sensible heat ratio.

Most air conditioners control temperature by cycling on and off and working at full power when the unit is on. Indoor humidity sensors however, do not even exist on most a/c units, and the sensible heat ratio depends on the indoor temperature and humidity, as well as the outdoor temperature. Therefore, for a room that has a specified SHR load, indoor and outdoor temperature, the indoor humidity is determined. Designers predict the typical SHR load that the unit will face at specified temperatures and then design the unit such that the indoor humidity at that SHR falls in the comfort zone.

Although designers aim for a 0.75 sensible heat ratio (SHR) in split systems at the standard ARI capacity rating condition a quick estimation of the loads for a house under different climates indicate that most loads actually have a much higher sensible load fraction. A 0.75 SHR is needed for the initial humidity pull down and to provide comfort in very humid climates, so there is room to increase the evaporator temperature under most other conditions. Raising the evaporator temperature would increase efficiency under those conditions where a high sensible load occurs, but would leave rooms with high latent load fractions too humid. Also, an a/c with a high SHR may not be capable of performing, at an acceptable rate, the initial humidity pull down needed in most climates.

14

One way around this problem is to design an air conditioner that operates at a higher evaporator temperature for maximum efficiency at most conditions, and has the capability to operate at a lower evaporator temperature to increase water removal in humid climates.

If the SHR load falls far below design condition, the indoor humidity would rise to a level outside the comfort zone, and it would be necessary to use dessicants or some other technology to change the indoor humidity without changing the air conditioner's SHR or the room's dry bulb temperature. One possible way to accomplish such a task, changing the evaporator blower speed and compressor speed, is analyzed in the following section.

4.3 Changing blower and compressor speed

The ACRC room a/c simulation computer model was used to simulate a split system and study the effects of blower speed on indoor humidity. The model was simulating a 3.0 ton Carrier unit that has a standard evaporator blower speed of 400 cfm/ton (nominal capacity). This unit has a thermal expansion valve, and all computer simulation runs assumed a constant 10 F of superheat in the evaporator. Blower speeds from 200 to 500 cfm/nominal ton were analyzed in this study. Effects of evaporator blower and compressor speed will be examined at a baseline climate condition of 75°F indoor temperature, 80°F outdoor temperature and 70°F outdoor dew-point temperature.

Both the sensible and latent heat loads can be considered constant when looking at short periods of time, and therefore the latent and sensible heat removal provided by the a/c unit must match those loads for steady state operating conditions. The ratio of sensible to latent heat transfer in the evaporator can be approximated by as:

(1)
$$\frac{Q_s}{Q_l} = \frac{h_a \times (T - T_s)}{h_a / C_{pm} \times (\omega - \omega_s(T_s))} \times \frac{A}{A_{wet}}$$

In this equation, h_a (the air side heat transfer coefficient) cancels out, and C_{pm} (the specific heat of the moist air at constant pressure) is close to one, so it can be neglected. Since T (the indoor temperature), ω (the indoor humidity) and A (the total evaporator area) are constants under steady state operation, the SHR is dependent on T_s (the evaporator surface temperature), and A_{wet} (the evaporator wet area)..

Equation 2 shows that SHR is a function of T_s and A_{wet}.

15

$$(2) \qquad SHR = \frac{Q_s}{Q_s + Q_l} = \frac{1}{1 + \frac{Q_l}{Q_s}(T_s, A_{wet})}$$

Figure 4.3.1 shows the effect of evaporator blower speed on the surface temperature of the evaporator at a baseline climate condition of 75°F indoor temperature, 80°F outdoor temperature and 70°F outdoor dew-point temperature. As the evaporator blower slows down from 500 to 200 cfm/ton, the air side heat transfer coefficient decreases causing a 9°F decrease in the evaporator surface temperature.
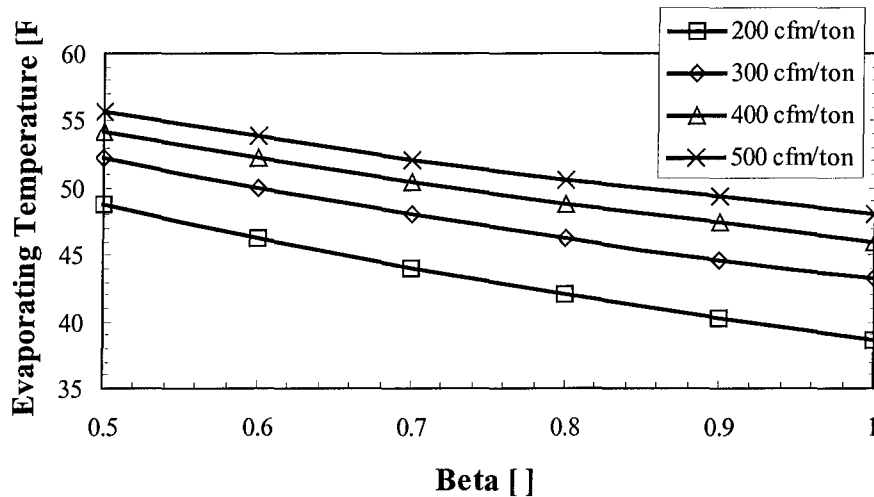
Figure 4.3.1: Evaporator average surface temperature vs. compressor and blower speeds.

The absolute humidity of the saturated air at the evaporator surface decreases, increasing the absolute humidity driving potential between the surface and the air passing the evaporator. However less air is going by the evaporator, so the overall effect, shown in Figure 4.3.2, is a 9% decrease in water removal rate or latent capacity.

16
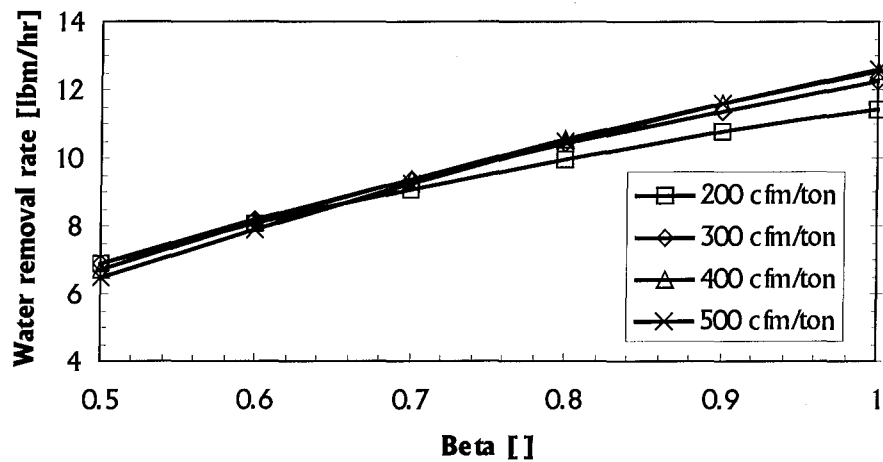
Figure 4.3.2: Water removal rate vs. compressor and blower speeds.

However there is also a sharp decrease (21%) in the unit's sensible capacity (Figure A.1.8), so the unit must run for longer periods of time (26% higher runtime fraction) to keep the indoor temperature constant, as shown in Figure 4.3.3. Therefore the system removes less humidity when it is running, but runs for longer periods, resulting in an overall higher water removal. All of this is reflected in the equilibrium steady state indoor relative humidity for the house; with the lower evaporator surface temperature, equilibrium is reached at a lower (and in most cases more comfortable) indoor wet bulb temperature.
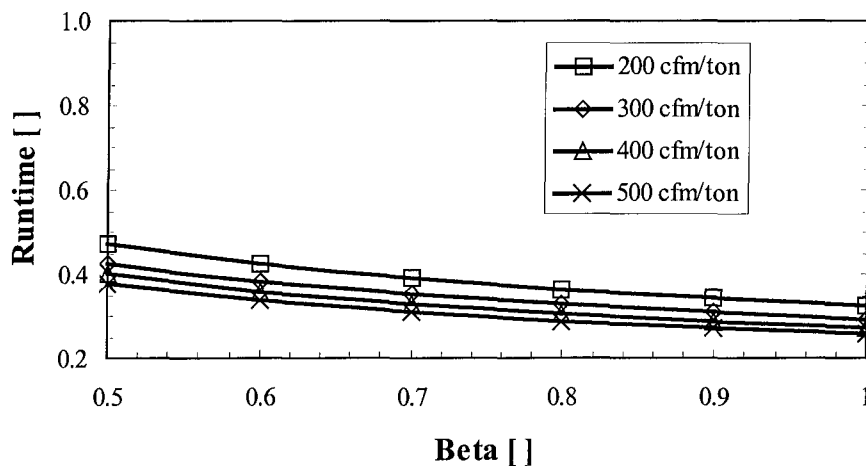
Figure 4.3.3: Runtime vs. compressor and blower speeds.

17

Figure 4.3.4 shows that this reduction in evaporator surface temperature causes a 6% reduction in indoor humidity, from 61 to 57% when blower speed is reduced from 500 to 200 cfm/ton. This indicates that a variable speed blower could be used to control, and significantly alter, the SHR of an a/c unit.
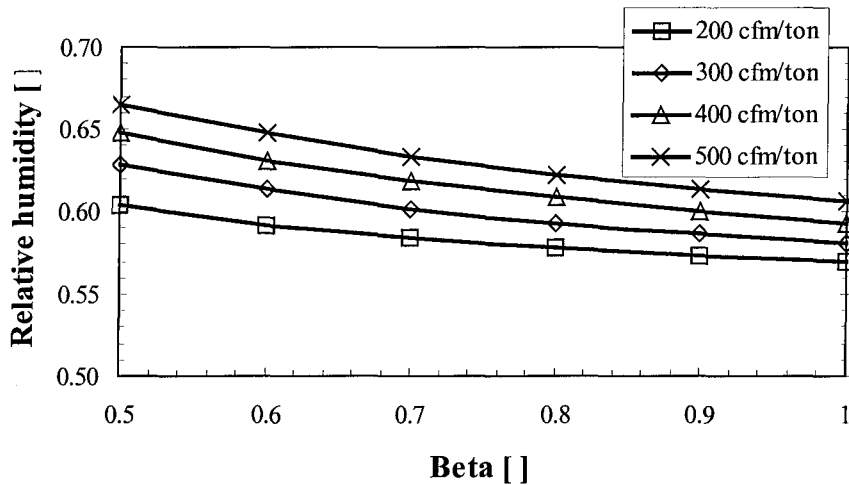
Figure 4.3.4: Indoor relative humidity vs. compressor and blower speeds.

This blower speed reduction also affects the unit's efficiency and power consumption. Decreasing the evaporator temperature decreases the heat exchanger effectiveness of the evaporator. On the other hand, the evaporator blower power consumption also decreases, so there is a positive overall effect of 22% in EER (Figure 4.3.5).
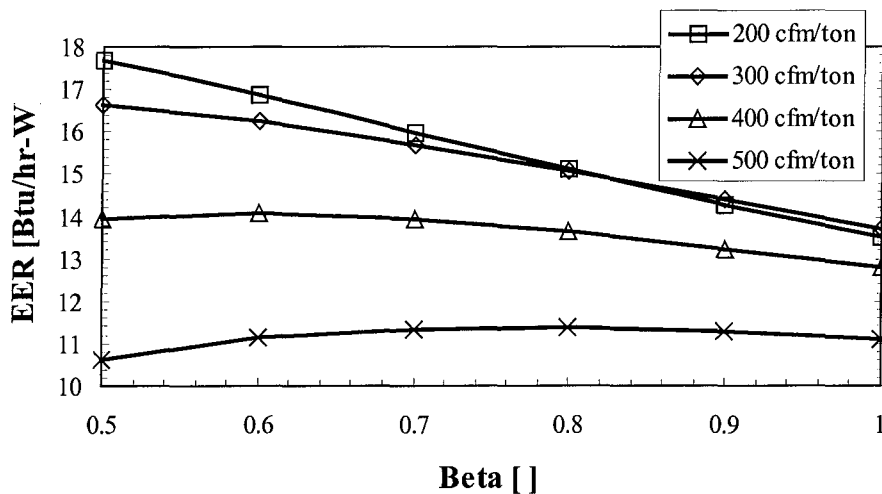
Figure 4.3.5: EER vs. compressor and blower speeds.

While slower blower speeds usually decrease power consumption, they also reduce capacity, therefore increasing runtimes (Figure 4.3.3). The overall effect of lower power consumption, and higher runtimes is best evaluated by looking at the total power input to the system averaged over a one hour period, which is calculated by multiplying the system power (compressor, evaporator blower, and condenser fan power) by runtime. As seen in Figure 4.3.6, this reduction of blower speed causes a 7% reduction in average power.
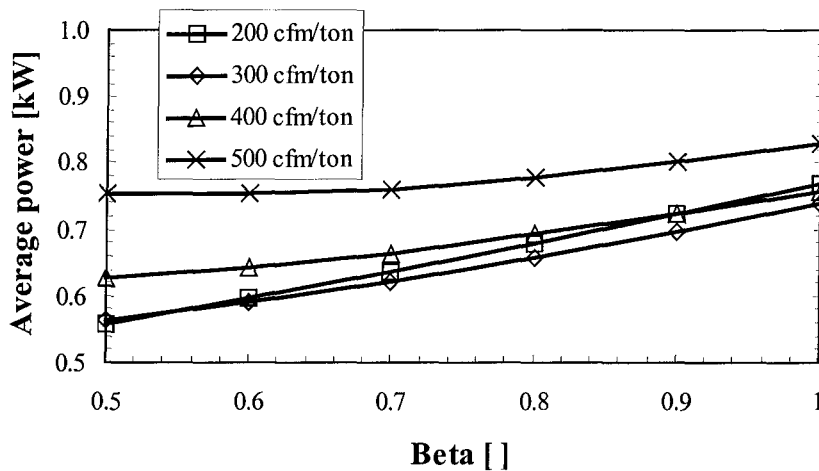
Figure 4.3.6: Average power vs. compressor and blower speeds.

Reducing the compressor speed however, has almost the opposite effect as slowing the blower speed. As beta decreases, the mass flow rate slows down, and the evaporating and condensing temperatures come closer together. Figure 4.3.4 shows that the same indoor humidity might be achieved with more than one compressor/blower speed combination. The natural question is which speed combination is better?

By the assumptions made in the model, for a specified inlet and outlet pressures, compressor power is directly proportional to compressor speed. Therefore, compressor speed has a greater effect on overall power consumption than blower speed. The following discussion considers halving the compressor speed (Beta = 0.5), and reducing evaporator blower from 500 to 200 cfm/ton.

Figure 4.3.1 shows the combined effects of evaporator blower speed and compressor speed on the surface temperature. As the evaporator blower slows down, the air side heat transfer coefficient decreases causing a decrease in the evaporator surface temperature. On the other hand, as the compressor slows down, the evaporator surface

19

temperature rises. The combined effect is a 1°F increase in evaporator surface temperature.

For the baseline climate, the reduction in compressor and blower speeds happens to cause an equal 45% reduction in both latent and sensible heat transfers, as shown in Figure 4.3.2 and Figure A.1.8, respectively. Therefore the system has to run for much longer runtimes (83% higher) to keep the house temperature constant (Figure 4.3.3), and there was no change in the equilibrium steady state indoor relative humidity (Figure 4.3.4) for the house. It was just a coincidence that the latent and sensible heat transfer reduced in the same proportion. This is not the case for other climate conditions, as shown in Section 4.7 and Appendix A.

Although there was no change in indoor humidity, this blower and compressor speed reduction significantly affects the unit's efficiency and power consumption. It is interesting to note that EER does not change monotonically with changes in either compressor or evaporator blower speeds. Reducing the compressor speed decreases both capacity and power consumption. The ratio of those two numbers (EER) is most sensitive to the EER gains achieved through blower speed reduction. The overall effect is a remarkable 59% increase in EER (Figure 4.3.5).

The most noticeable effect of slowing the compressor and the evaporator blower speed is the increase in runtimes (Figure 4.3.3), and accompanying decrease in power consumption. Combining these two effects, Figure 4.3.6 shows a 32% reduction in average power. The combination of low compressor and blower speeds ensures the lowest average power consumption for this climate condition, but it is accompanied by only a slight decrease in indoor humidity, or comfort.

4.4 Effect of cycle lengths

Figure 4.3.3 shows how the runtime fraction increases as blower and compressor speeds are reduced. This effect is expected because reducing the blower speed increases the air-side heat transfer resistance and therefore decreases the evaporator sensible heat transfer. Since most of the heat transfer in the evaporator is sensible, this effect more than offsets any increases in latent heat transfer. Slowing the compressor decreases refrigerant mass flow, which reduces both latent and sensible heat transfer. As the heat transfer decreases, longer runtimes are needed to keep the indoor temperature constant.

This increase in runtime has a positive effect in water removal as shown experimentally by Porter (1999). When the unit shuts off, some of the water vapor that has condensed on the evaporator surface will re-evaporate into the house, specially if the evaporator blower is left on when the compressor turns off (economizer mode). At the beginning of the on-cycle, the water vapor condenses on the evaporator surface before it starts dripping into the condensate removal pan. Therefore shorter runtimes mean less actual water removal from the building. In extreme cases, when runtimes are short, the unit turns off before water starts dripping from the evaporator, and the water that has condensed in the evaporator surface re-evaporates into the room, causing a zero effective water removal.

4.5 Capillary tube versus thermal expansion valve systems

Thermal expansion valves (TXV) maintain a constant superheat, which forces the (dry) superheated area of the evaporator to remain nearly constant. In most operating conditions simulated in this study, the 2-phase zone of the evaporator is fully wet, therefore the wetted area fraction of the evaporator is nearly constant as shown in Figure 4.5.1.
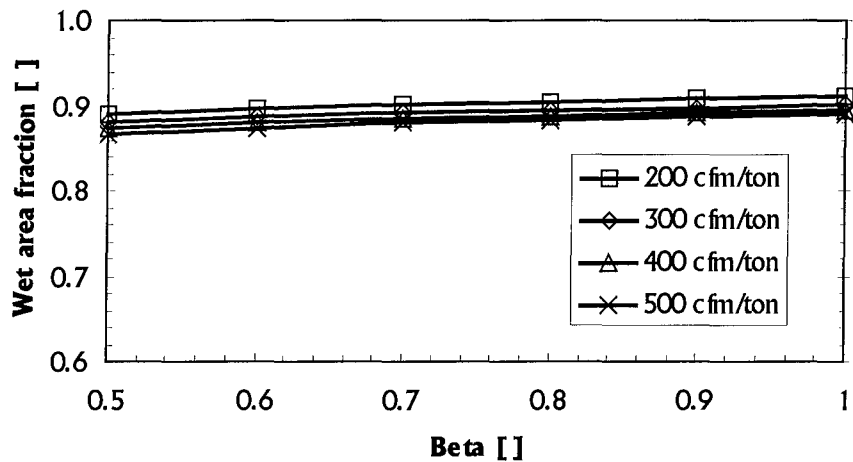

Figure 4.5.1: Wetted area fraction vs. compressor and blower speeds.

At lower indoor humidities, the leading edges of the fins may be dry. Figure 4.5.2 shows the wetted area fraction for a partially wet evaporator for a warm and dry climate (75 °F indoor temperature, 95 °F outdoor dry-bulb temperature and 60 °F wet-bulb

temperature). Section 5 of Appendix A describes this climate condition in greater detail. The changing wetted area fraction accentuates the slope of the curves presented here. At this condition, the evaporator surface temperature reduction obtained by reducing blower speed not only increases the delta in absolute humidity driving potential between evaporator surface and air, but also helps prevent the evaporator surface from going dry. Therefore, when the wetted area fraction is changing, reducing blower speed has a larger effect on the indoor humidity than usual. Reducing the compressor speed on the other hand, decreases the evaporator wetted area fraction, so it has a negative effect on comfort.

A system with a capillary tube would always have a changing wetted area fraction since superheat varies with compressor and blower speed.
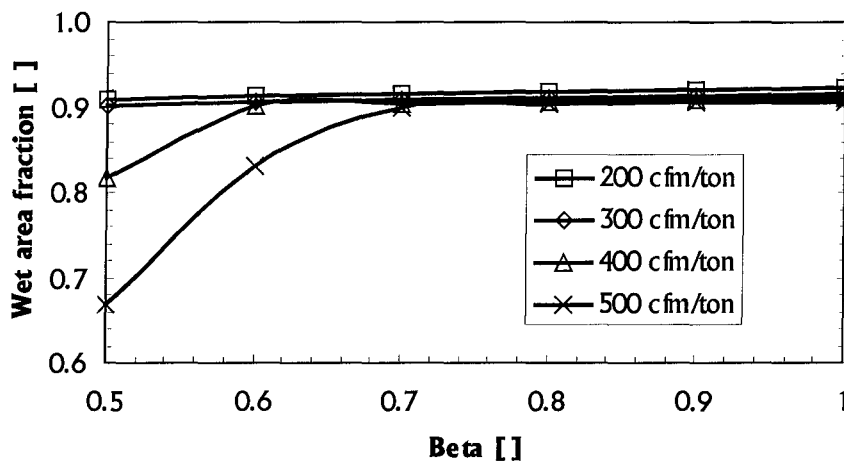

Figure 4.5.2: Wetted area fraction vs. compressor and blower speeds for a partially-wet evaporator.

4.6 Effect of infiltration

Sections 9 and 10 of Appendix A show the effects of having a loosely sealed and tightly sealed house with the same conditions described above. Infiltration is the main source of latent load, but it contributes only a moderate part of the sensible load. Therefore, the effect of a tightly sealed house versus a regular house is like that of a lower outdoor humidity. With lower infiltration rates, less moisture enters the house,

leading to a lower indoor humidity. Also, the unit will have a lower power consumption since it does not have to condense and remove as much water from the indoor environment. A loosely sealed house has the opposite effect, a higher indoor humidity and power consumption.

Assuming that the indoor relative humidity varies linearly with outdoor dew-point (a crude assumption) between the cool-dry and baseline climate conditions described in Appendix A, equivalent effects on the indoor humidity were interpolated for the tightly sealed house. A tightly sealed house versus a normally sealed house has the same effect on indoor humidity as a 3°F decrease in the outdoor dew-point temperature. Similar calculations show that a loosely sealed house has the same effect as a 3°F increase in dew-point temperature or an incremental 1.3 lbm/hr of water.

4.7 Effect of outdoor climate

Appendix A shows the effect of changes on both outdoor dry-bulb temperature and dew-point temperature. Dry-bulb temperature has a strong effect on sensible load, while dew-point temperature affects latent load only. Since sensible load is the main load component, dry-bulb temperature changes have a much stronger effect on the overall system and indoor environment than dew-point temperature. Higher dry-bulb temperature imply in higher overall loads which lead to a higher power consumption, and a higher SHR which leads to a lower indoor humidity.

Dew-point temperatures have a direct effect on indoor humidity and power consumption. With a higher outdoor humidity, more water vapor will infiltrate into the indoor environment, and the unit has to consume more energy to try to remove it.

Chapter 5

Conclusion

The results presented in Chapter 4 show how indoor humidity can be lowered by decreasing the evaporator air flow rate, because the fin temperatures are reduced and remove more condensate. In a moderate climate condition (75°F indoor temperature, 80°F outdoor temperature and 70°F outdoor dew-point temperature), indoor relative humidity can be reduced from 61 to 57% by reducing the blower speed from 500 cfm/ton to 200 cfm/ton. In a warmer climate (75/95/70), a similar blower speed reduction causes the indoor relative humidity to fall from 55 to 48%. In a hot climate (75/110/70) an even greater reduction is observed, from 54 to 45%. These and other climate conditions are shown in Appendix A.

In addition to the extra comfort, system power input, averaged over the on/off cycles, decreases for most climate conditions with this blower speed reduction. At high refrigerant mass flow rates, the refrigerant-side heat transfer resistance is small so most of the ΔT is on the air side. Therefore, reducing the blower speed increases the overall ΔT, thereby reducing evaporating temperature and degrading system performance. On the other hand, blower power has a cubic reduction with blower speed, so the net result is usually a decrease in average power usage. In a moderate climate (75/80/70), average power drops from 0.83 to 0.77 kW, a 7% decrease in power usage for a 6% reduction in humidity, or increase in comfort. In a warmer (75/95/70) climate, a smaller decrease in average power is observed, from 1.97 to 1.91 kW, or a 3% decrease in average power, with a 12% gains in comfort or reduction in indoor humidity. In a hot (75/110/70) climate, there is a small (0.5%) increase in average power from 3.64 to 3.66 kW, and a large reduction in indoor humidity, 16%.

The EER of the system is a strong function of compressor speed. Modest reductions in refrigerant mass flow rate increase EER by utilizing the heat exchangers for longer runtimes at lower ΔT's, resulting in a smaller temperature lift. However due to the degradation of refrigerant-side heat transfer coefficient at these lower mass fluxes, the refrigerant-side ΔT is a larger fraction of the total, so the effect of blower speed is diluted. The energy savings due to reduction of blower power are a greater fraction of the total system power at lower compressor speeds. Overall, the system runs more efficiently but

for a longer time, removing the same sensible load and latent load, and preventing short-cycling that would increase indoor humidity. The net effect is more comfort and no increased energy use. It has been shown that short cycles prevent latent load removal, therefore increasing indoor humidity. Not accounting for this effects, in our baseline climate (75/80/70) halving the compressor speed and reducing the blower speed from 500 to 200 cfm/ton has a negligible effect in indoor humidity, and reduces average power 33% from 0.83 to 0.56 kW.

These simulations show that by using a variable speed compressor and blower can prevent short-cycling, and improve indoor humidity control with little or no sacrifice in system efficiency.

Appendices

Appendix A

Effects of climate

This appendix contains graphs for a range of climates. The same scale is maintained for most of the graphs, however, some variables vary widely with climate conditions, so the minimum and maximum vary to reflect this.

A.1 Baseline climate

This is the baseline climate shown in Chapter 4. It considers a house with regular infiltration (as described in the ASHRAE Fundamentals) in a moderately humid climate (80°F outdoors and 70°F dew-point). Some of these graphs were also presented in Chapter 4. As explained in Chapter 4, "average power" refers to the power used by the unit (both compressor and blowers) to keep steady state conditions times the on-time fraction of the unit.
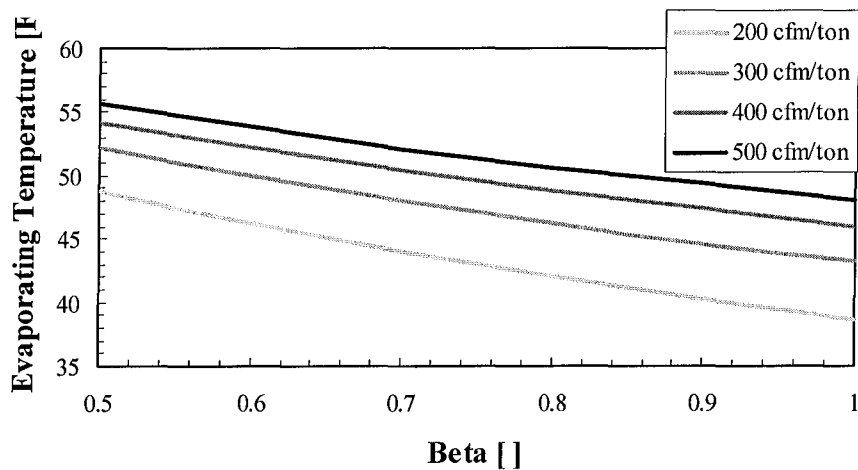
Figure A.1.3: Evaporating temperature, baseline climate.
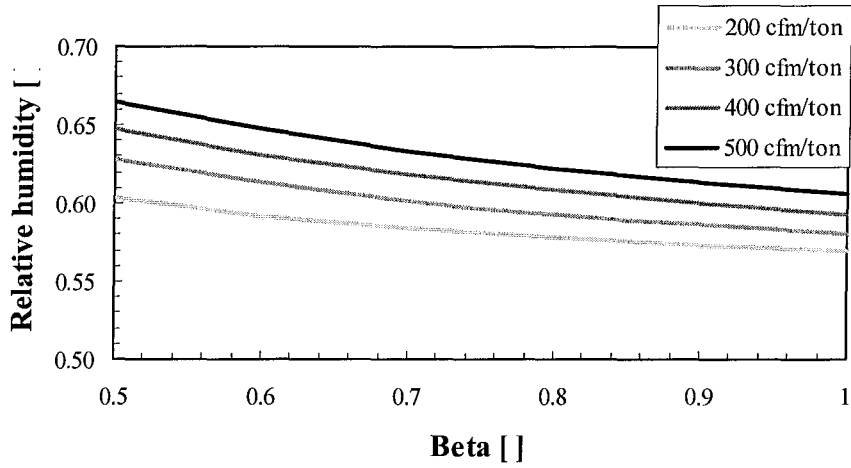
Figure A.1.4: Relative humidity, baseline climate.
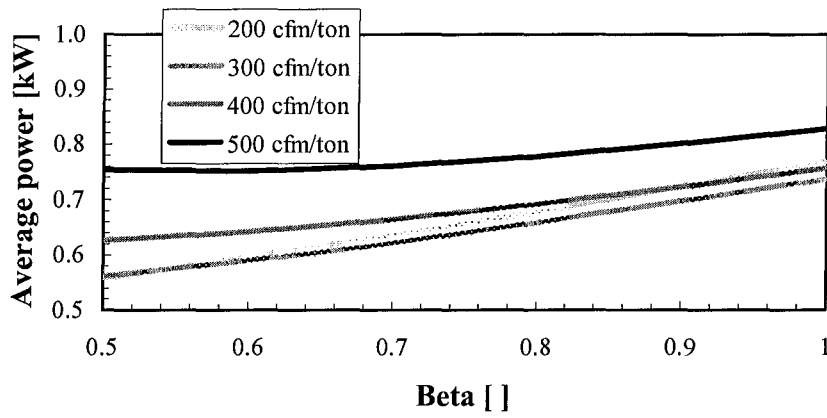

Figure A.1.5: Average power, baseline climate.
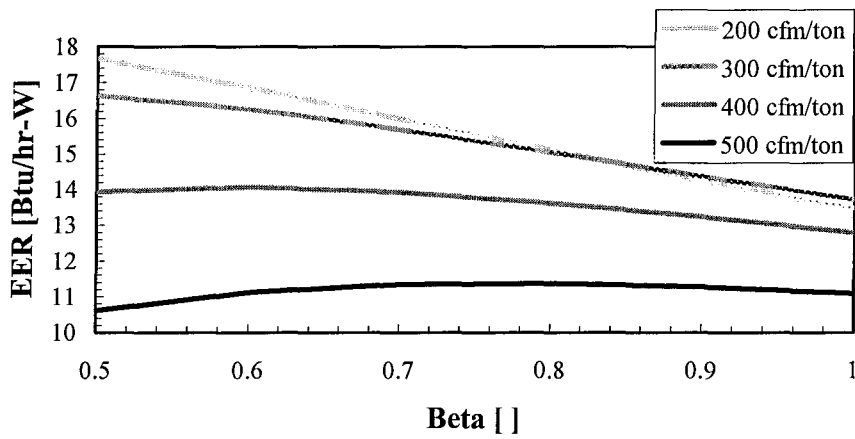

Figure A.1.6: EER, baseline climate.
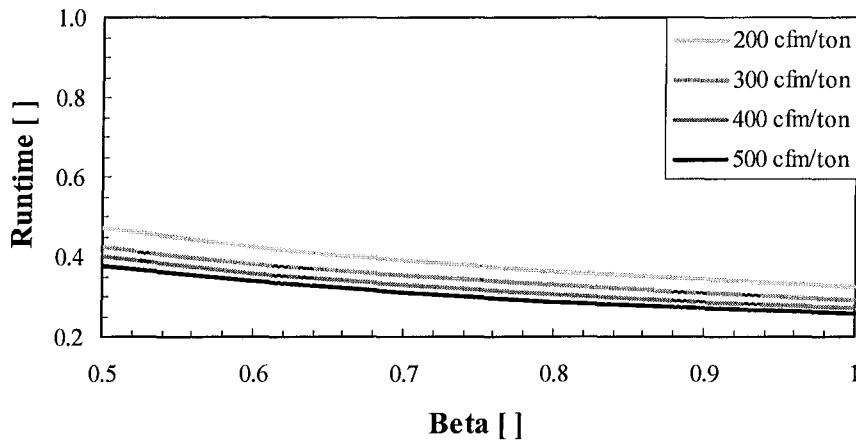
Figure A.1.7: Runtime, baseline climate.
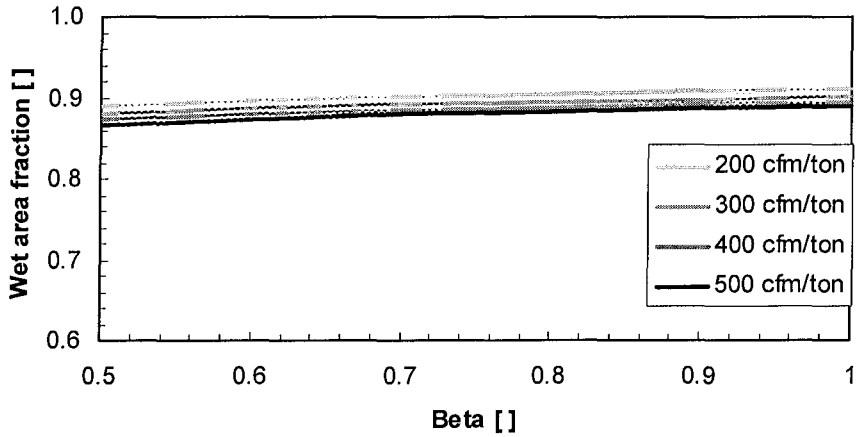
Figure A.1.8: Wetted area fraction, baseline climate.
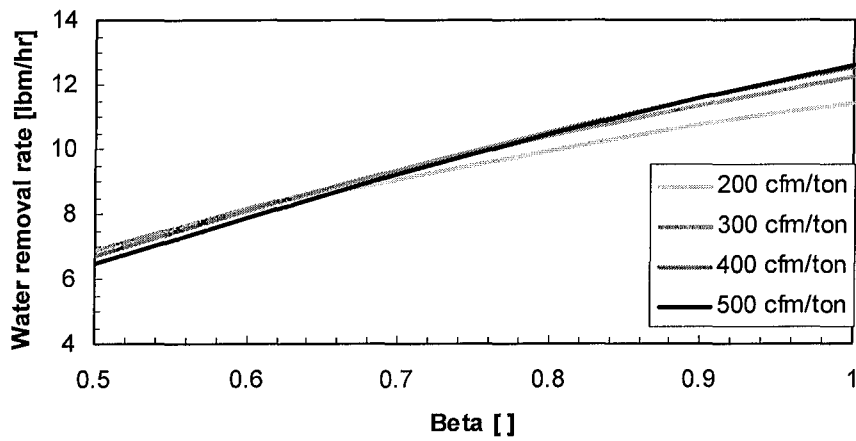

Figure A.1.9: Water removal rate, baseline climate.
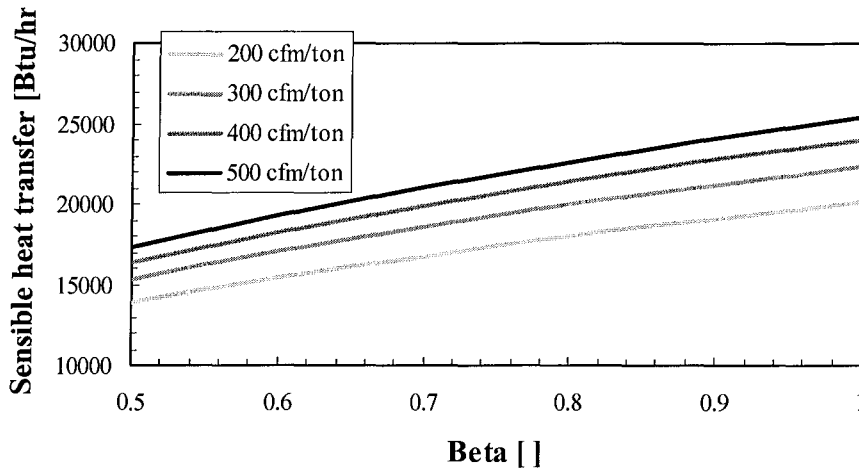
Figure A.1.10: Sensible heat transfer, baseline climate.
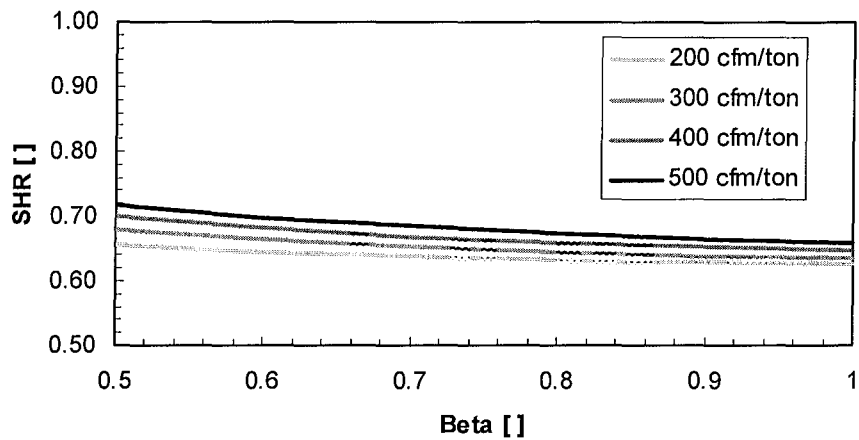
Figure A.1.11: Sensible heat ratio, baseline climate.

A.2 Cool-dry climate

This graphs show the results of a simulation of a cool (80 °F outdoors) and dry (60°F dew-point) climate. The house has the same infiltration as described in Chapter 3, and is kept at 75°F indoors.

Because this a dryer climate than the baseline, less water infiltrate (the biggest source of humidity), and the house is dryer. The average power is also less than the baseline since the unit does not have to work as hard to remove water from the house. Other variables like EER, wetted area fraction, etc have curves similar to the baseline curves with minor vertical shifts.
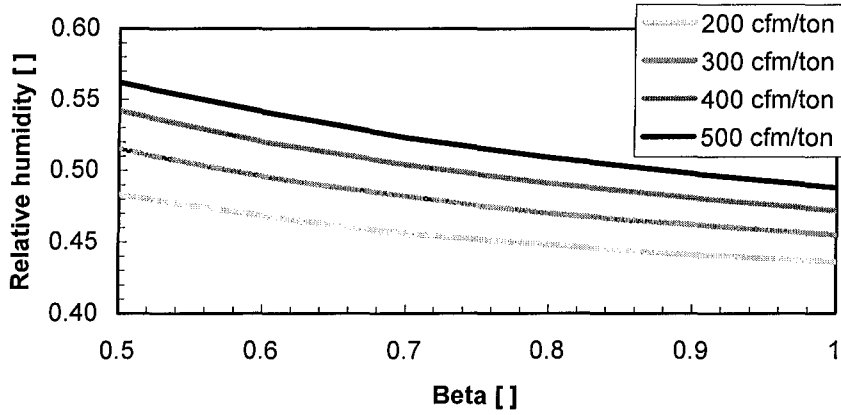
Figure A.2.1: Relative humidity, cool-dry climate.
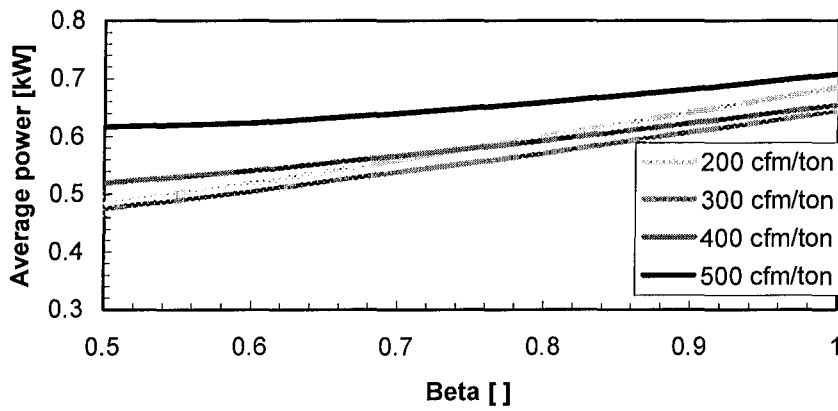
Figure A.2.2: Average power, cool-dry climate.
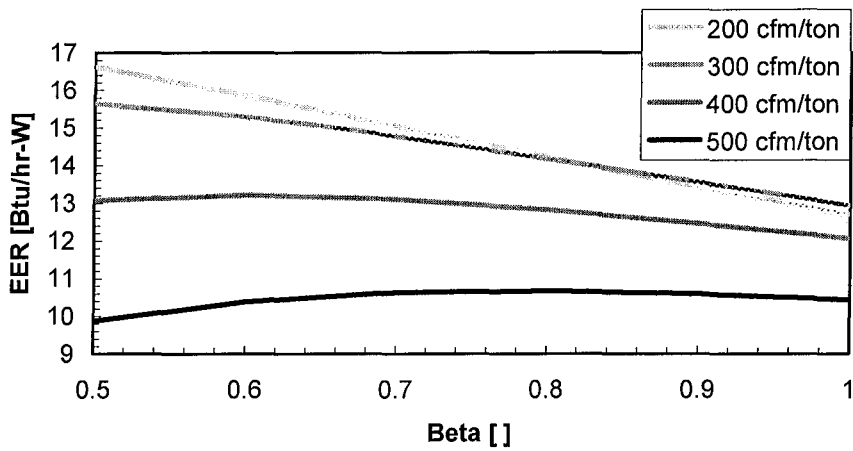
Figure A.2.3: EER, cool-dry climate.
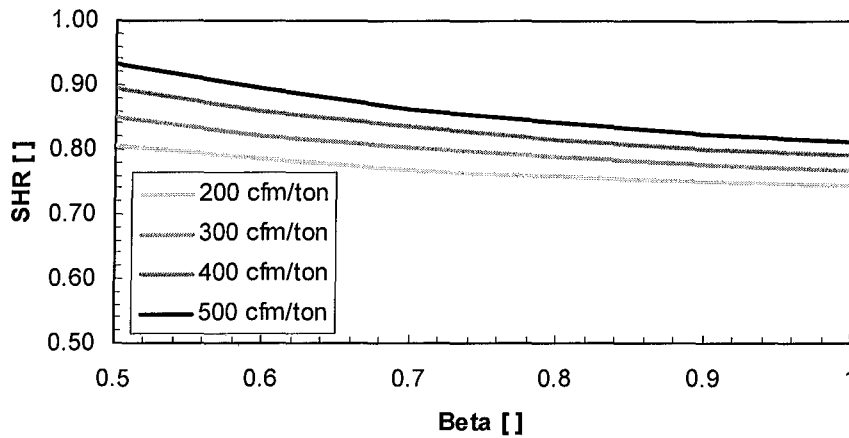
Figure A.2.4: Sensible heat ratio, cool-dry climate.

A.3 Cool-humid climate

This graphs show the results of a simulation of a cool (80 °F outdoors) and

humid(80°F dew-point) climate. The house has the same infiltration as described in

Chapter 3, and is kept at 75°F indoors.

Because this is a more humid climate than the baseline, more water infiltrates

making the house more humid. The unit has to work harder to remove the extra water

from the house, therefore the average power is more than the baseline. Other variables

like EER, wetted area fraction, etc have curves similar to the baseline curves with minor

vertical shifts.
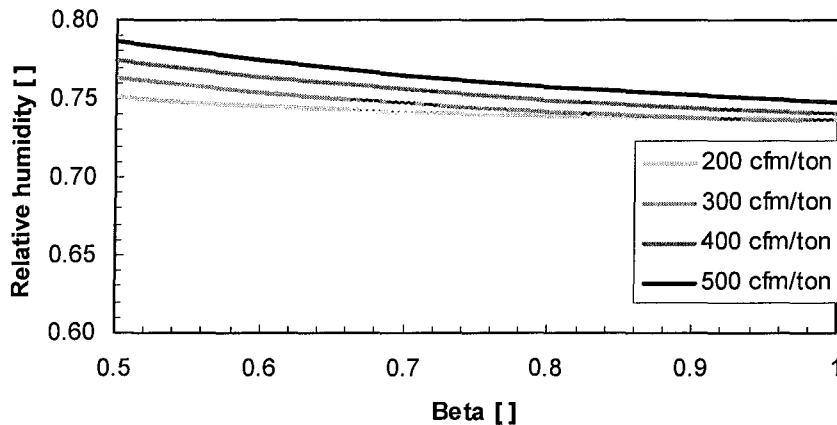
Figure A.3.1: Relative humidity, cool-humid climate.
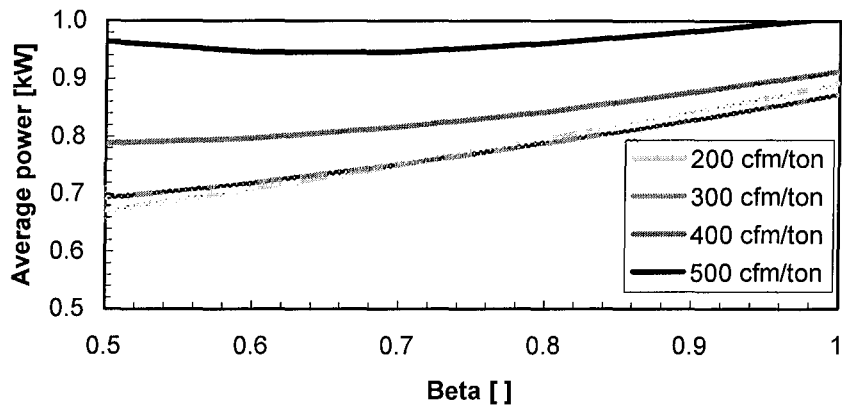
Figure A.3.2: Average power, cool-humid climate.
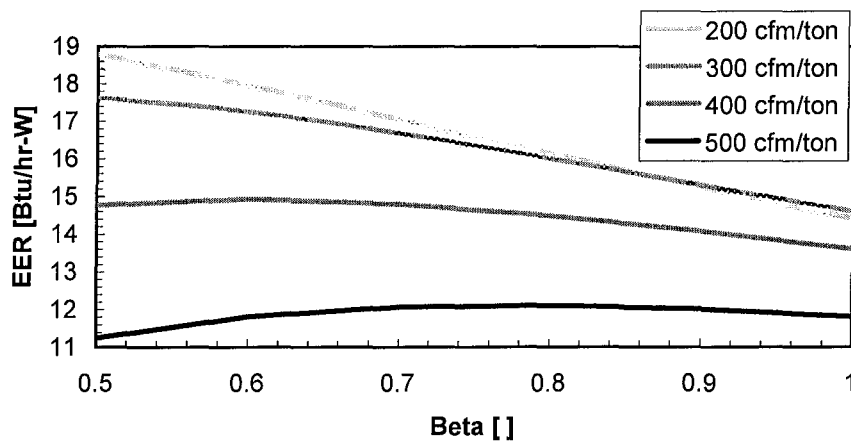

Figure A.3.3: EER, cool-humid climate.
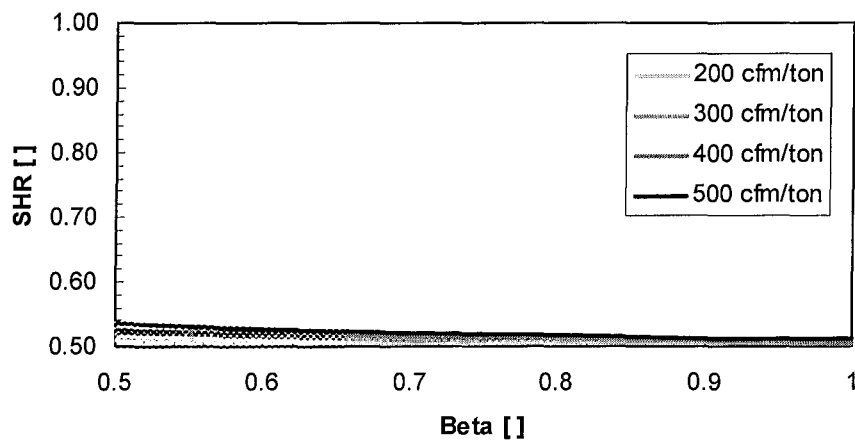
Figure A.3.4: Sensible heat ratio, cool-humid climate.

A.4 Warm-moderate humidity climate

This graphs show the results of a simulation of a warm (95 °F outdoors) and moderate humidity (70°F dew-point) climate. The house has the same infiltration as described in Chapter 3, and is kept at 75°F indoors.

The higher outdoor temperature significantly increases the sensible load on the unit. This higher load forces the unit to work longer, and therefore remove water for longer periods of time. With the unit working longer, more water is removed, and the indoor humidity goes down. Therefore the water removal rate goes down. This gives the unit a higher SHR than before. The higher temperature between difference indoors and outdoors also contributes to a higher infiltration and therefore higher latent load. However, this is only a minor effect, and the overall SHR for the load increases. Therefore, new equilibrium condition for the house will have a lower indoor humidity even though the water removal rate decreased. As expected, the average power for the unit is higher due to the extra sensible load.
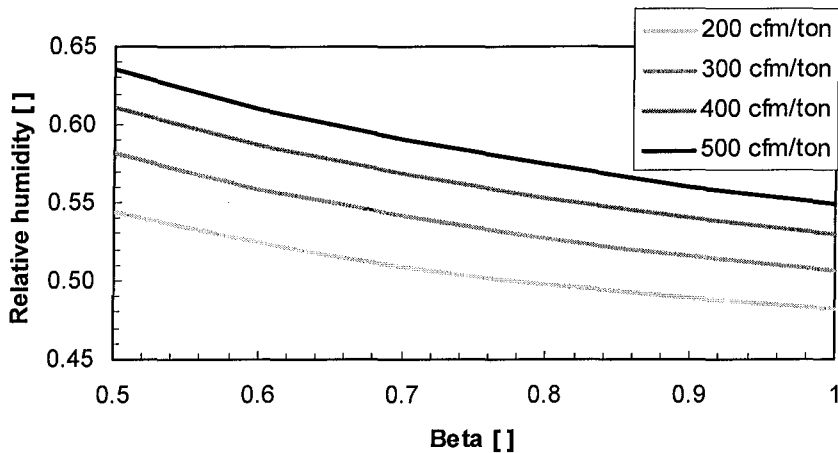
Figure A.4.1: Relative humidity, warm-moderate humidity climate.
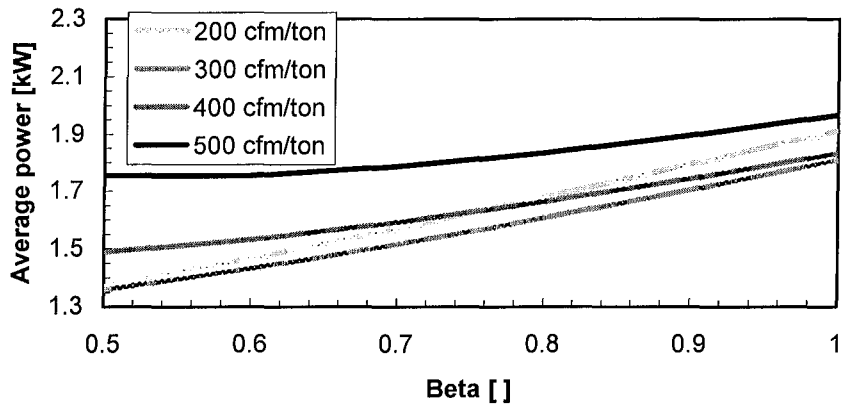
Figure A.4.2: Average power, warm-moderate humidity climate.
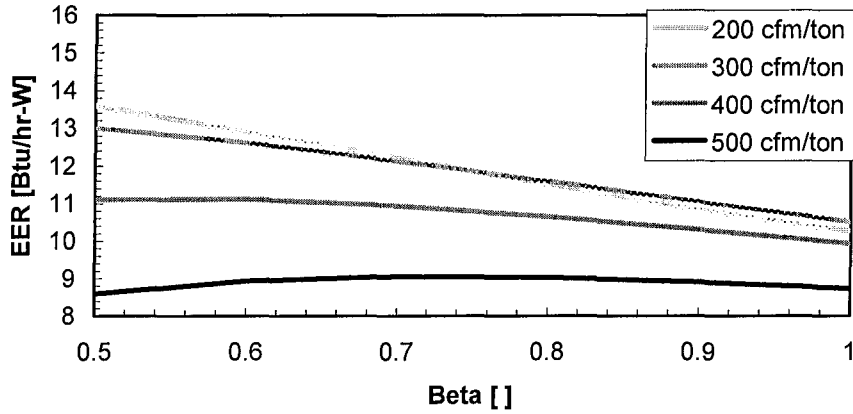
Figure A.4.3: EER, warm-moderate humidity climate.
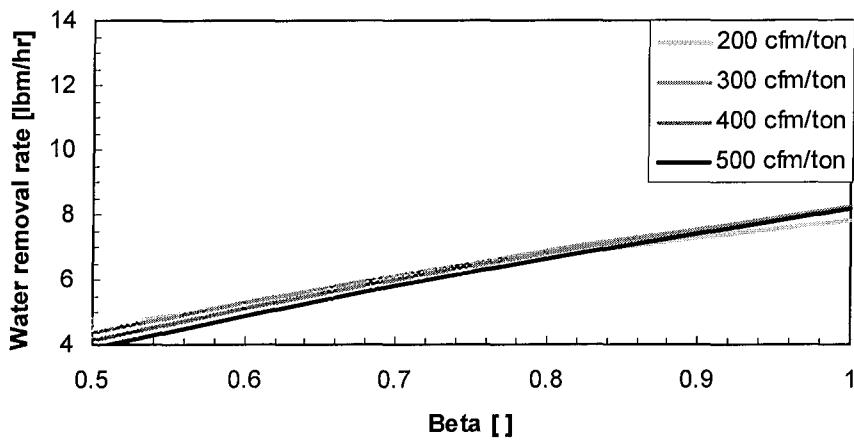
Figure A.4.4: Water removal rate, warm-moderate humidity climate.
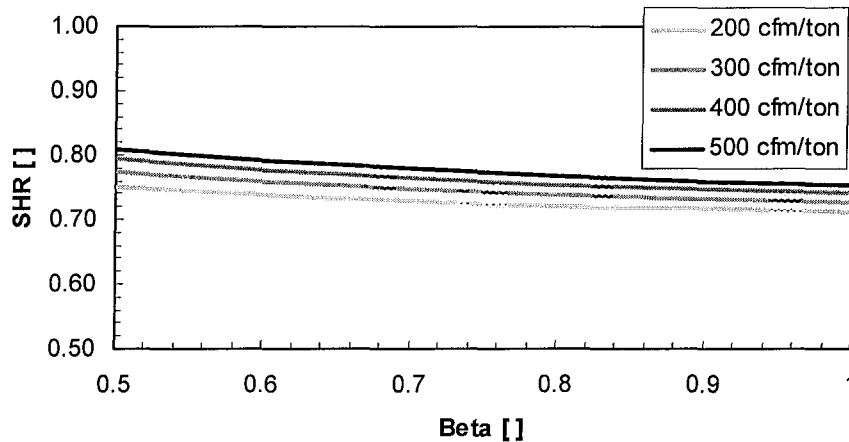
Figure A.4.5: Sensible heat ratio, warm-moderate humidity climate.

A.5 Warm-dry climate

This graphs show the results of a simulation of a warm (95 °F outdoors) and dry (60°F dew-point) climate. The house has the same infiltration as described in Chapter 3, and is kept at 75°F indoors.

This climate presents a very similar behavior to the warm-moderate humidity climate presented above. However, since it is dryer, it has a lower indoor humidity and average power for the same reasons presented in Section A.2.

At low compressor speeds, the unit has a partially wet evaporator, which create a slope in the nearly constant wetted area fraction. This discontinuity is reflected by a somewhat abrupt change in slope in the indoor humidity curve, and most of the other curves.
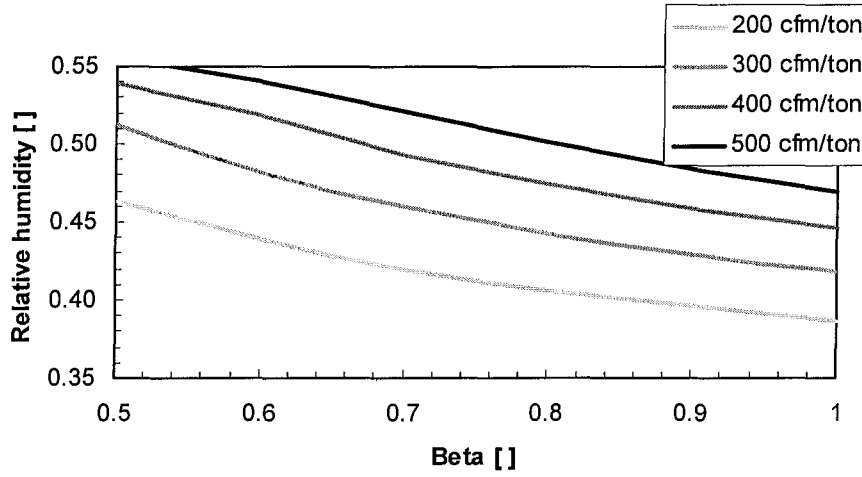
Figure A.5.1: Relative humidity, warm-dry climate.
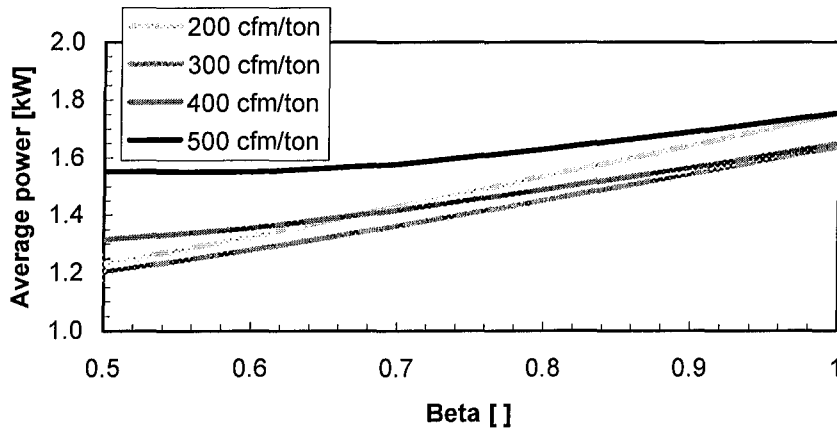
Figure A.5.2: Average power, warm-dry climate.
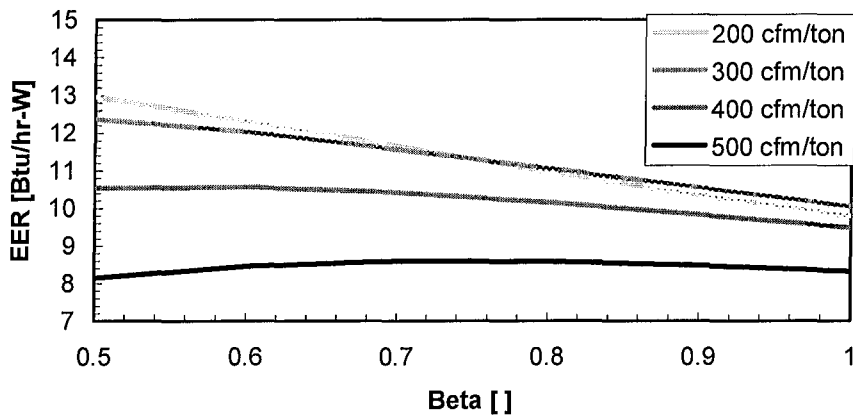
Figure A.5.3: EER, warm-dry climate.
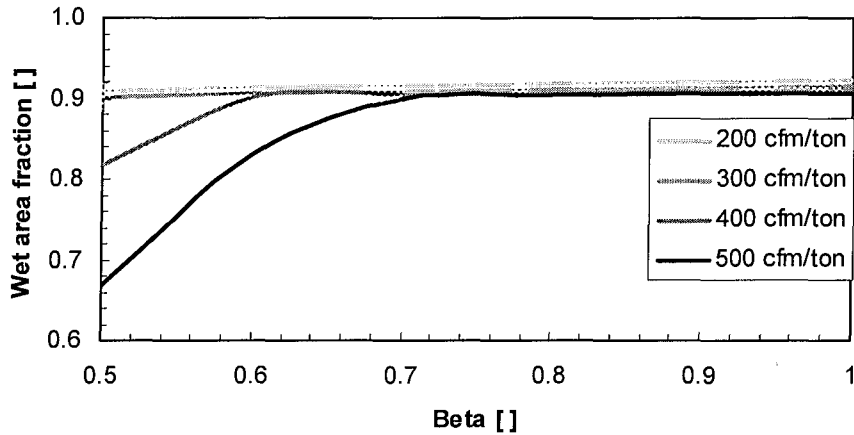
Figure A.5.4: Wetted area fraction, warm-dry climate.
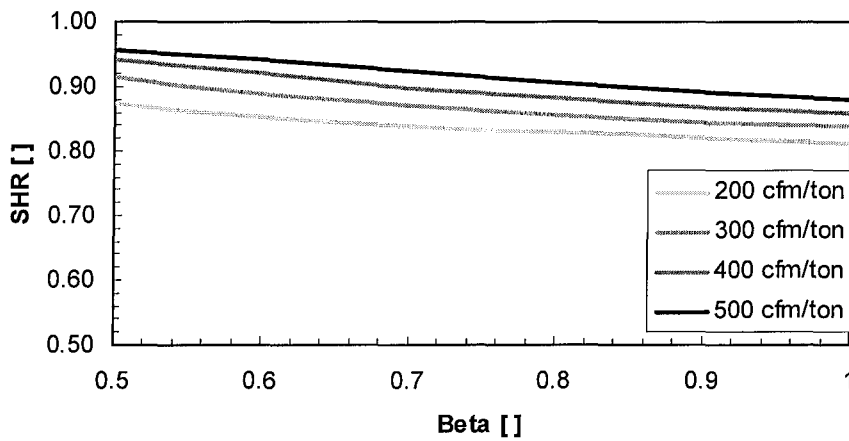
Figure A.5.5: Sensible heat ratio, warm-dry climate.

A.6 Warm-humid climate

This graphs show the results of a simulation of a warm (95 °F outdoors) and humid (80°F dew-point) climate. The house has the same infiltration as described in Chapter 3, and is kept at 75°F indoors.

This climate presents a very similar behavior to the warm-moderate humidity climate presented above. However, since it is more humid, it has a higher indoor humidity and average power for the same reasons presented in Section A.3.
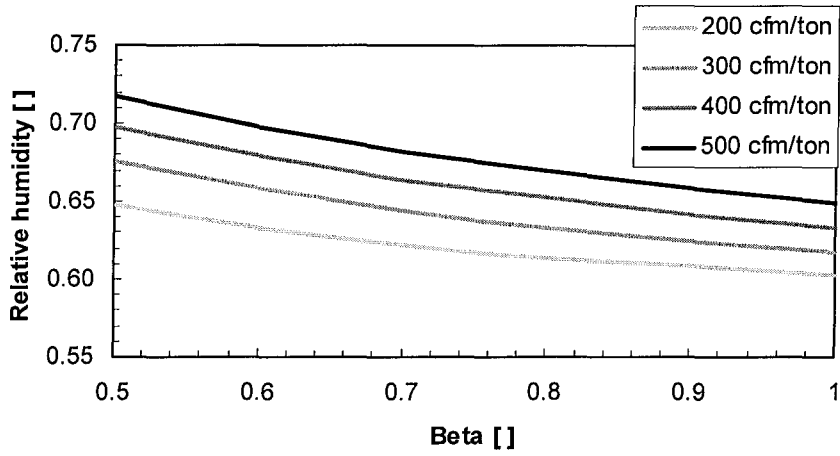
Figure A.6.1: Relative humidity, warm-humid climate.
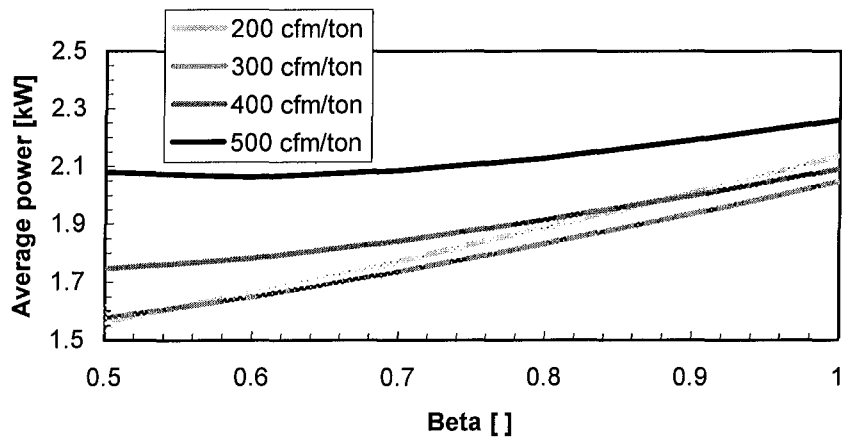
Figure A.6.2: Average power, warm-humid climate.
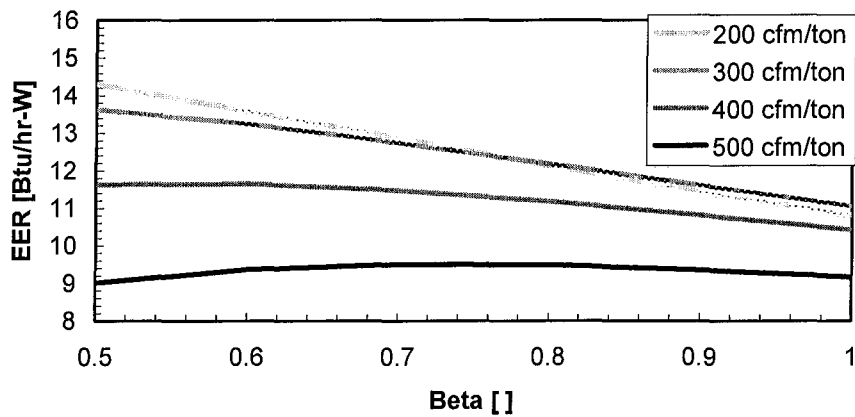
Figure A.6.3: EER, warm-humid climate.
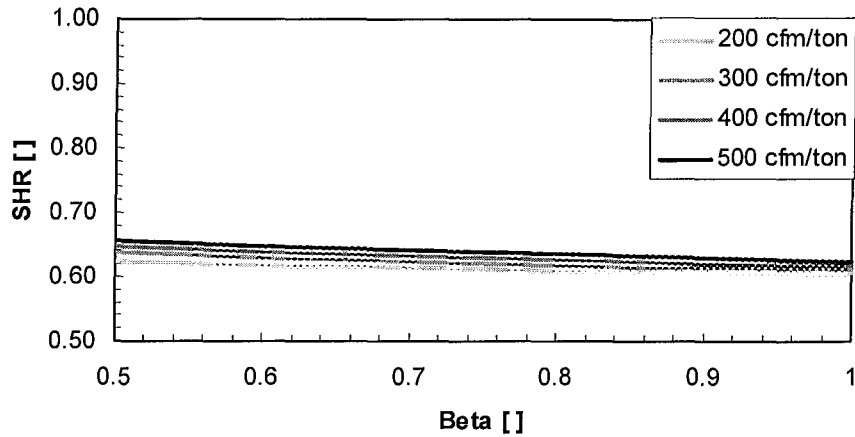
Figure A.6.4: Sensible heat ratio, warm-humid climate.

A.7 Hot-moderate humidity climate

This graphs show the results of a simulation of a hot (110 °F outdoors) and moderate humidity (70°F dew-point) climate. The house has the same infiltration as described in Chapter 3, and is kept at 75°F indoors.

Similar effects to those explained in Section A.4 make for a lower indoor humidity (even with a lower water removal rate) and a higher average power than for a warm climate.

The high loads also lead the model to predict runtime fractions higher than one, when blower and compressor speeds are reduced too far. This means that the unit would not be able to keep the house at 75°F under these extreme conditions.
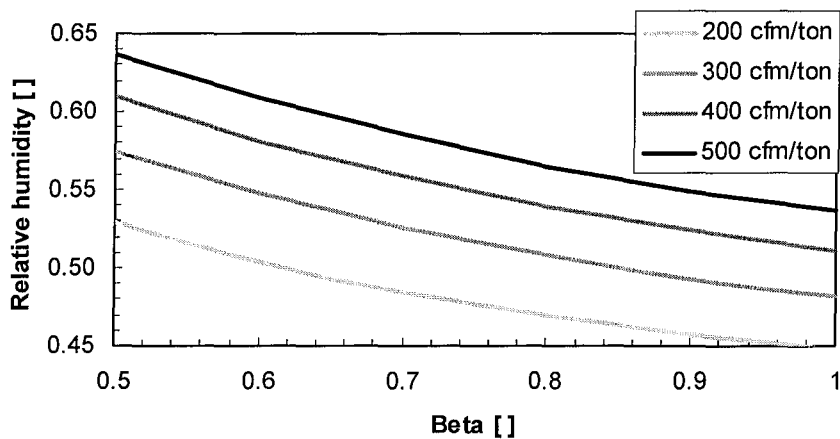
Figure A.7.1: Relative humidity, hot-moderate humidity climate.
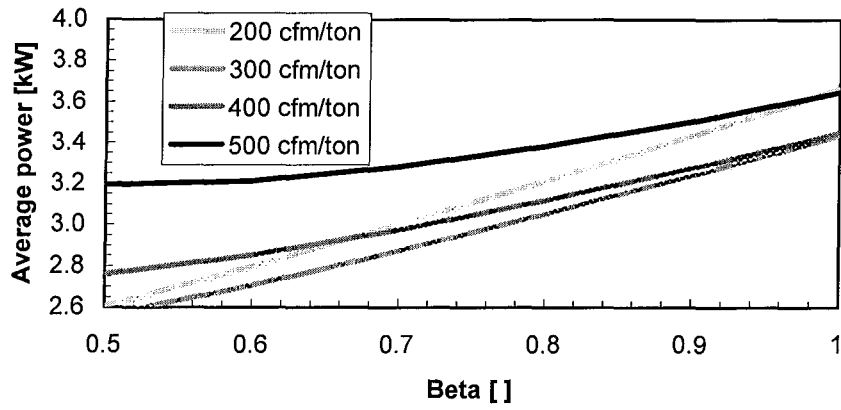
Figure A.7.2: Average power, hot-moderate humidity climate.
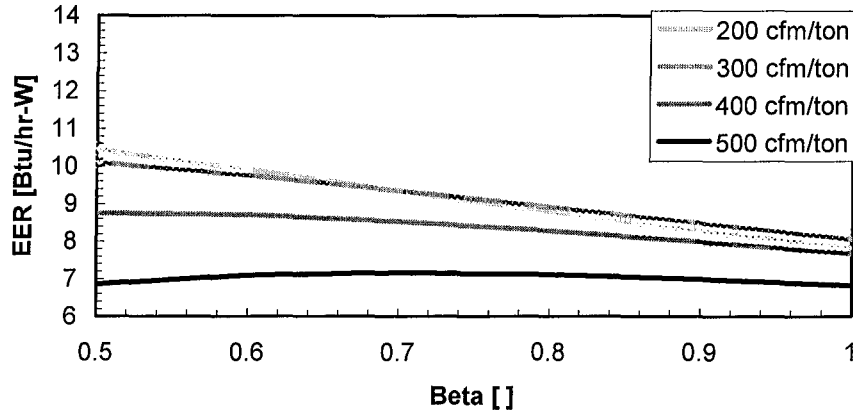

Figure A.7.3: EER, hot-moderate humidity climate.
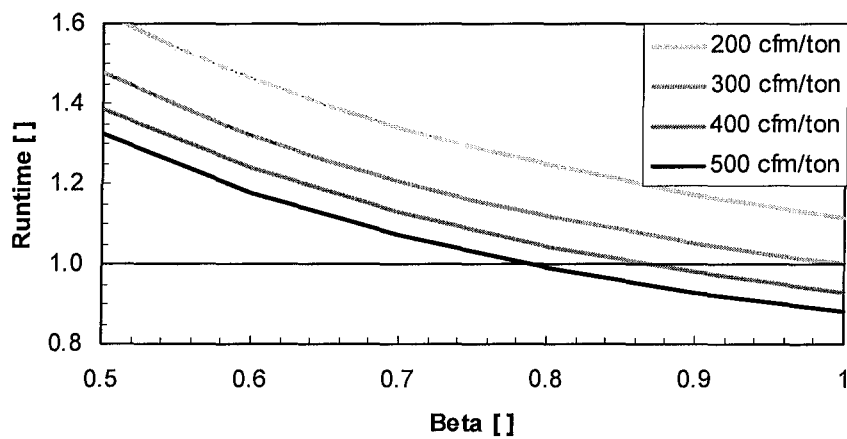


Figure A.7.4: Runtime, hot-moderate humidity climate.

41
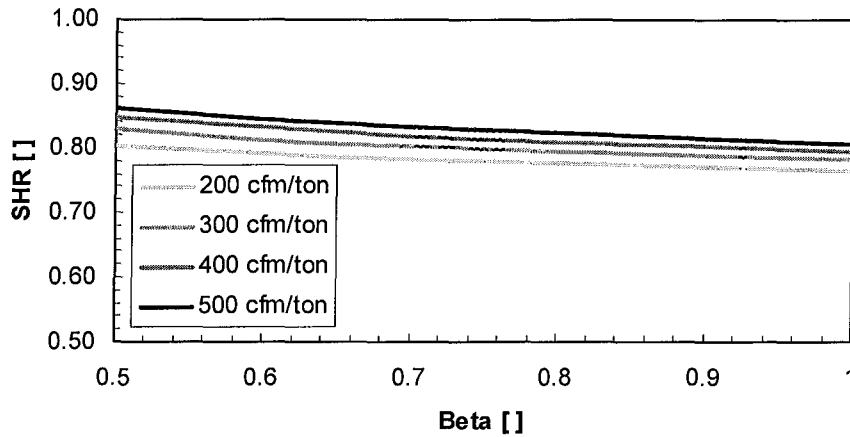
Figure A.7.5: Sensible heat ratio, hot-moderate humidity climate.

A.8 Hot-humid climate

This graphs show the results of a simulation of a hot (110 °F outdoors) and humid (80°F dew-point) climate. The house has the same infiltration as described in Chapter 3, and is kept at 75°F indoors.

This climate is similar to the hot-moderate humidity climate presented above, with a higher indoor humidity and average power due to the extra humidity infiltrating the house. Again, the model to predict runtime fractions higher than one when blower and compressor speeds are reduced, meaning that the unit would not be able to keep the house at 75°F under these extreme conditions.
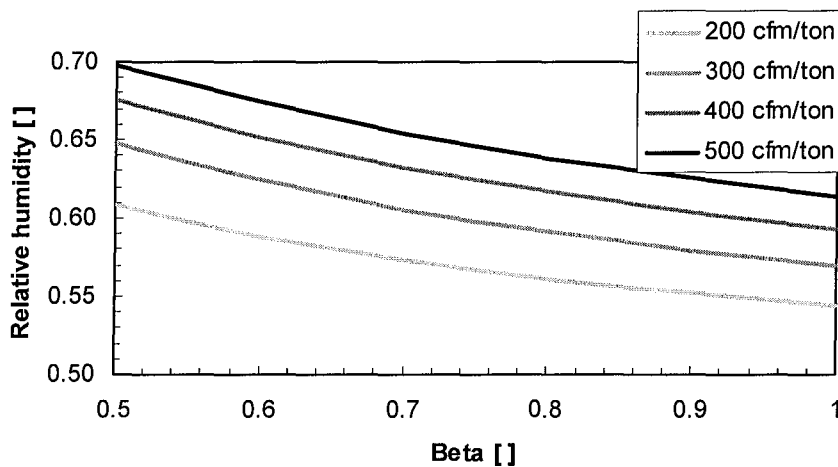
Figure A.8.1: Relative humidity, hot-humid climate.
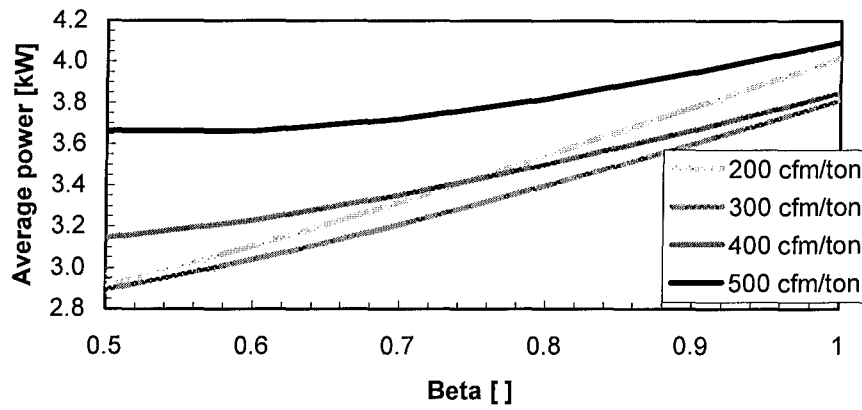
Figure A.8.2: Average power, hot-humid climate.
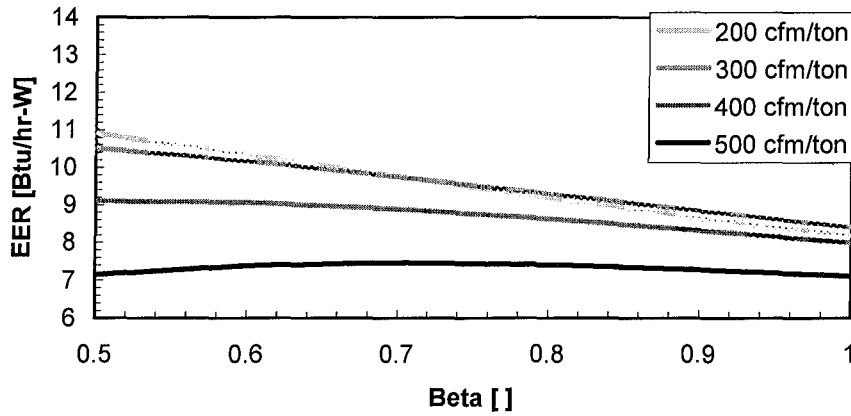
Figure A.8.3: EER, hot-humid climate.
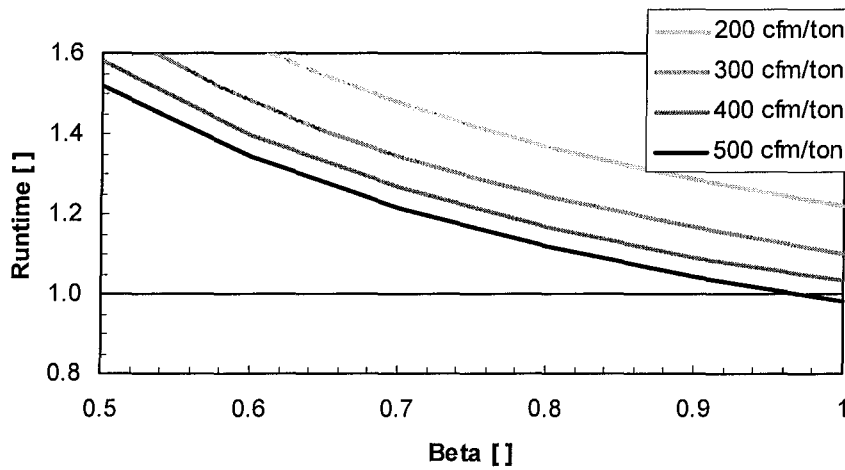
Figure A.8.4: Runtime, hot-humid climate.

43
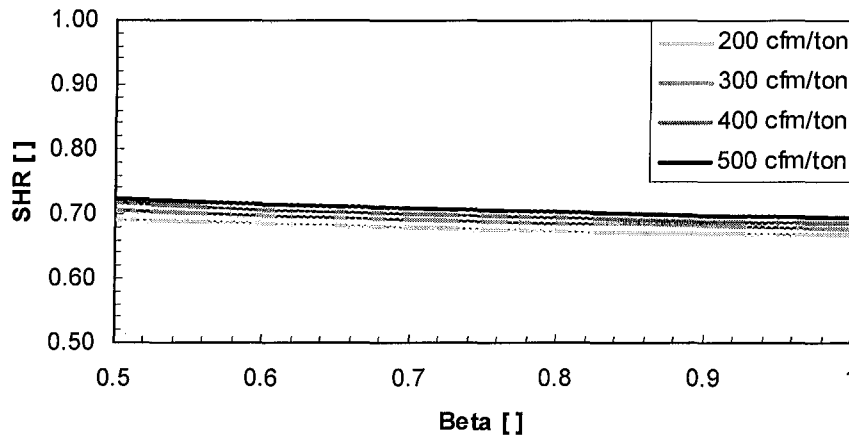
Figure A.8.5: Sensible heat ratio, hot-humid climate.

A.9 Loose house

This graphs show the results of a simulation of the baseline cool (80 °F outdoors) and moderate humidity (70°F dew-point) climate. However this simulates a loosely sealed house (as defined in the ASHRAE Fundamentals), and therefore a higher infiltration. The house is kept at 75°F indoors.

The effect of this extra infiltration is somewhat similar (although less dramatic) to that of a humid climate. The load on the unit has a lower SHR, and therefore the house has a higher indoor humidity. The extra load also forces a higher average power, and water removal rate.
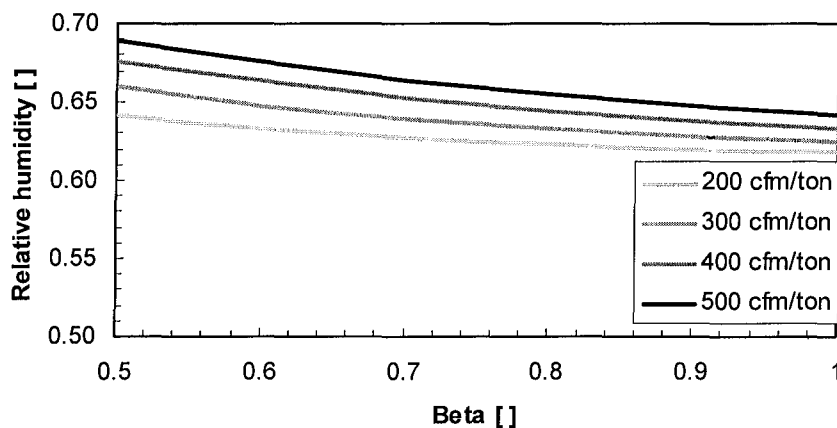
Figure A.9.1: Relative humidity, baseline climate in a loosely sealed house.
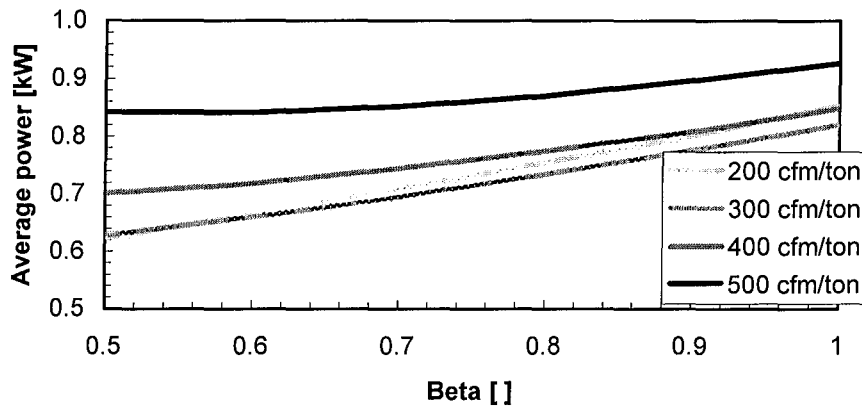
Figure A.9.2: Average power, baseline climate in a loosely sealed house.
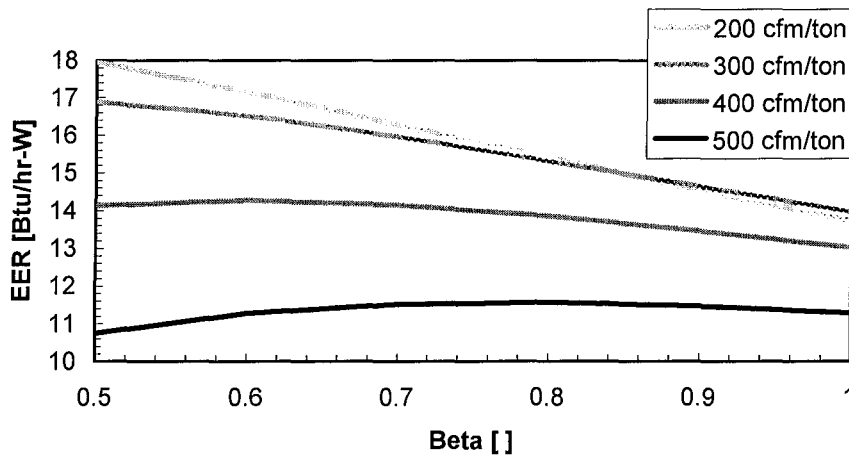
Figure A.9.3: EER, baseline climate in a loosely sealed house.
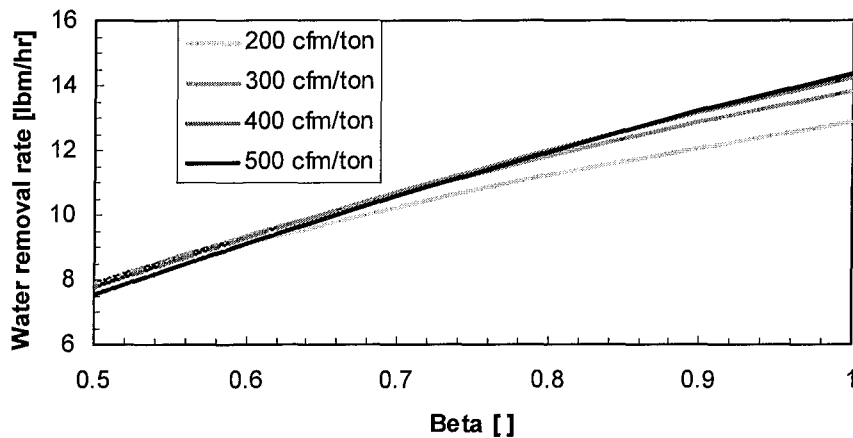
Figure A.9.4: Water removal rate, baseline climate in a loosely sealed house.
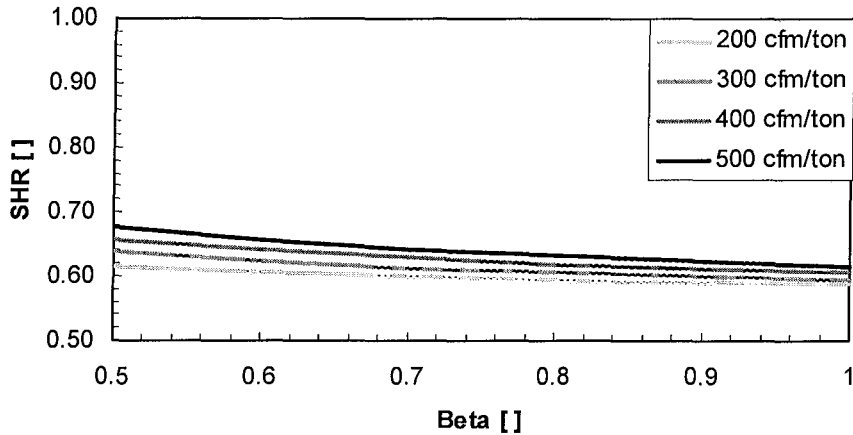
Figure A.9.5: Sensible heat ratio, baseline climate in a loosely sealed house.

A.10 Tight house

This graphs show the results of a simulation of the baseline cool (80 °F outdoors) and moderate humidity (70°F dew-point) climate. However this simulates a tightly sealed house (as defined in the ASHRAE Fundamentals), and therefore a lower infiltration. The house is kept at 75°F indoors.

Like the loosely sealed house is similar to a more humid climate, a tightly sealed house is similar to a dryer climate. The smaller latent load on the unit causes a lower indoor humidity, lower average power, and lower water removal rate.
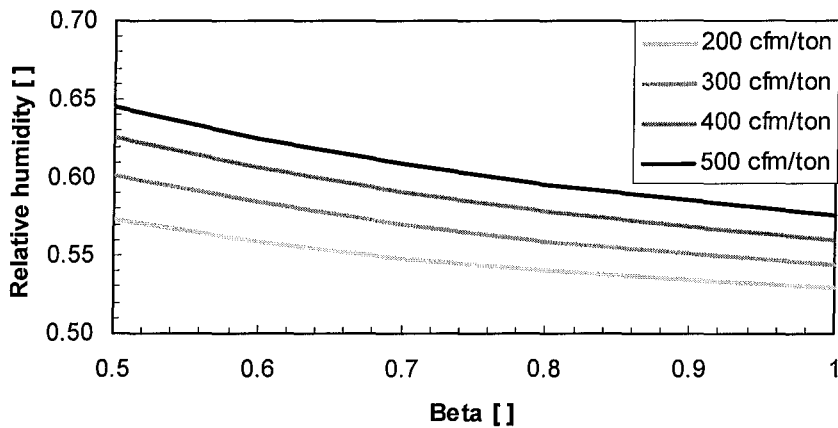
Figure A.10.1: Relative humidity, baseline climate in a tightly sealed house.
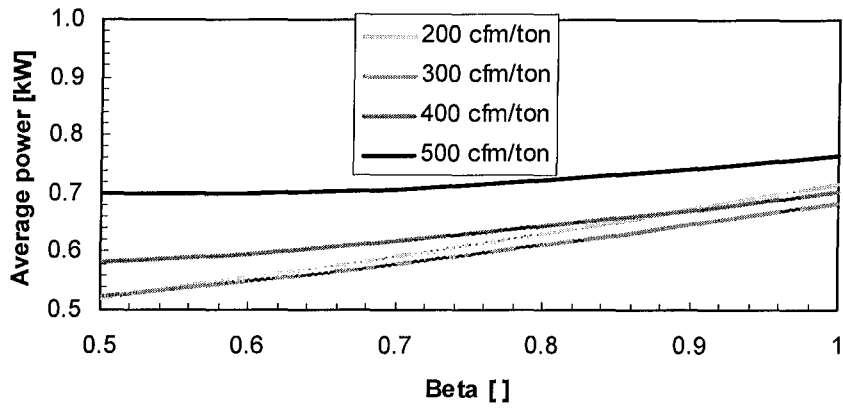
Figure A.10.2: Average power, baseline climate in a tightly sealed house.
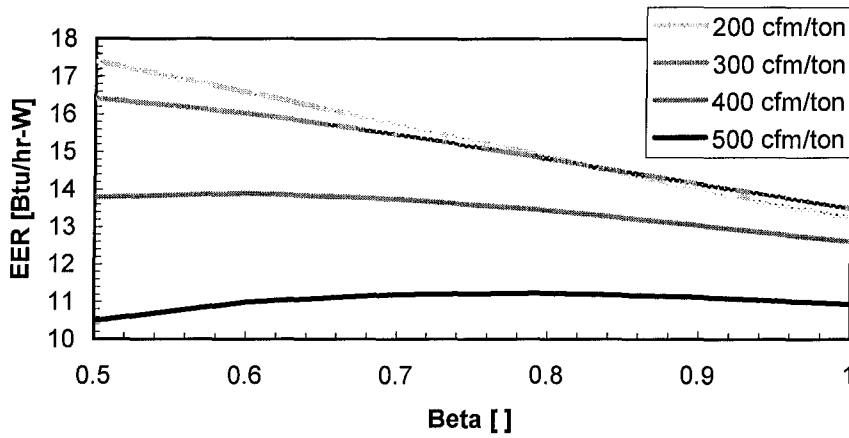
Figure A.10.3: EER, baseline climate in a tightly sealed house.
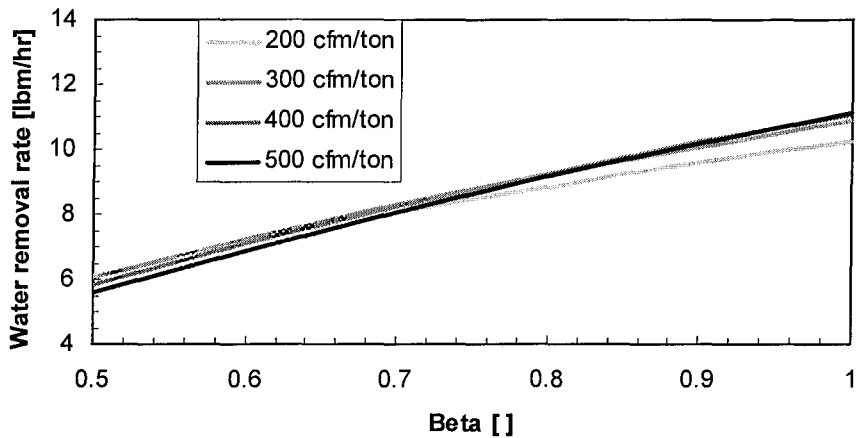
Figure A.10.4: Water removal rate, baseline climate in a tightly sealed house.
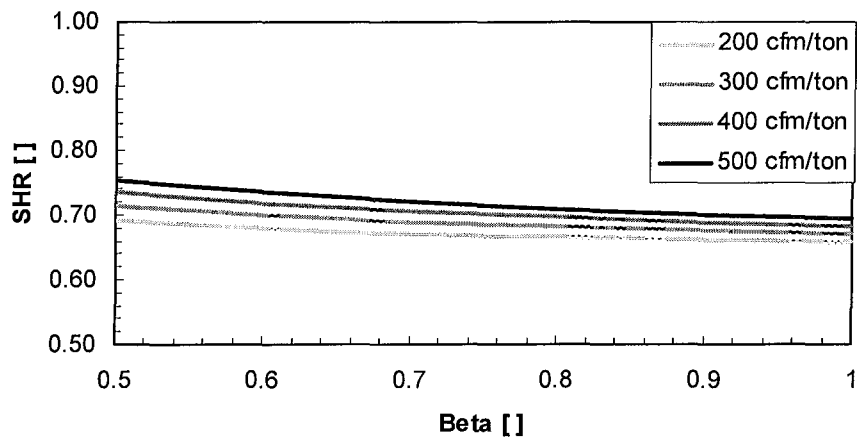
Figure A.10.5: Sensible heat ratio, baseline climate in a tightly sealed house.

Appendix B

Indoor Room Capacity

B.1 Introduction

In replacing a 1.5 ton window a/c unit with a 2.5 ton split a/c unit, one of the biggest concerns was the range of testing conditions the facility would be able to achieve with the split system, and what should be modified to increase the range of testing conditions if they prove to be inappropriate. The increased capacity of the new test unit meant that the test facility would have to add more heat and moisture into the indoor room, and to remove more heat and moisture from the outdoor room to maintain steady state conditions.

Appendix C discusses the issues related to the outdoor room capacity, and this appendix discusses the issues related to the indoor room capacity.

B.2 Indoor Room Capacity

Past experience with the 1.5 ton unit showed was that the facility could not handle high indoor humidity test conditions. At those conditions, a high moisture output is required from the humidifier. However, since the humidifier is not perfectly insulated, it also provides sensible heat to the indoor room. At high indoor relative humidities, the sensible heat output from the humidifier was greater than the 1.5 ton unit's sensible heat removal capacity.

The 2.5 ton unit, however, would be able to remove the sensible heat from the humidifier, and still demand a heat load from the furnace. Since the furnace power is the only variable used to control the temperature in the indoor room, it is essential that the furnace operates at all test conditions. The first analysis of the indoor room capacity indicated that with the new unit, the indoor side of the test facility would be able to handle the full test matrix, including wet points that could not be done with the old unit.

$y = 0.2548x - 1.0813$
$R^2 = 0.9953$
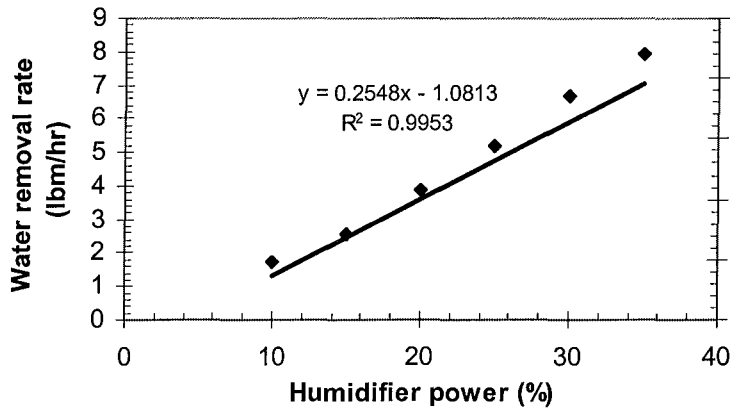
Figure B.2.1 shows a curve fit for the water output versus the humidifier percentage output using humidifier data from the test facility. Assuming a maximum power output of 8000 Watts as rated by the manufacturer, the humidifier power was correlated to the steam output of the humidifier. The latent heat output of the humidifier is equal to the humidifier water output times the latent heat of vaporization. The humidifier sensible heat output is equal to the total humidifier heat output minus the latent heat. A computer simulation model calculated the water removal rate and evaporator load for the unit under several conditions. The difference between the evaporator capacity and the humidifier load is equal to the required furnace output. The furnace percentage power is equal to the actual furnace power divided by the maximum furnace power (10 kW as provided by the manufacturer).

Table B.2.1 shows the normalized furnace and humifier outputs required to keep the indoor room at steady state at several indoor relative humidities at 80° F indoors, and 82° F outdoors. Table B.2.2 shows the same results at 80° F indoors, and 95° F outdoors.

$y = 0.2548x - 1.0813$
$R^2 = 0.9953$
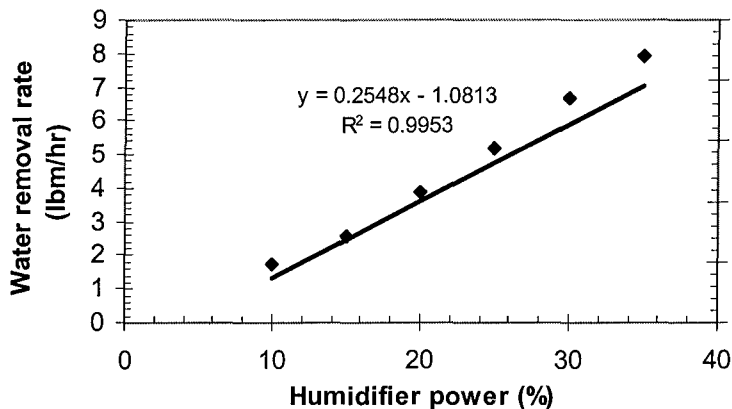
Figure B.2.1: Water removal rate versus humidifier power.

RhaiE	Qevap	MWR	Hum Power %	Furnace %
0.50	31600	7.8	35	64
0.55	32500	10.2	44	60
0.60	33400	12.4	53	56
0.65	34300	14.5	61	52
0.70	35200	16.6	69	48
0.75	35900	18.5	77	44
0.80	36700	20.4	84	40
0.85	37300	22.0	91	37
0.90	37900	23.6	97	34
0.95	38400	24.9	102	31

Table B.2.1: Humidifier and furnace output for several indoor relative humidities at 80/82.

RhaiE	Qevap	MWR	Hum Power %	Furnace %
0.50	39600	13.9	59	69
0.55	40900	17.0	71	63
0.60	42200	19.9	82	58
0.65	43400	22.6	93	53
0.70	44500	25.2	103	48

Table B.2.2: Humidifier and furnace output for several indoor relative humidities at 80/95.

Appendix C

Outdoor Room Capacity

C.1 Introduction

In replacing a 1.5 ton window a/c unit with a 2.5 ton split system, one of the biggest concerns was the range of testing conditions the facility would be able to achieve. It was necessary to determine what should be modified in order to increase the range of testing conditions. The increased capacity of the new test unit meant that the test facility would have to add more heat and moisture into the indoor room, and to remove more heat from the outdoor room to maintain steady state conditions.

Appendix β discusses the issues related to the indoor room capacity, and this appendix discusses the issues related to the outdoor room capacity.

C.2 Outdoor Room Capacity

Removing more heat from the outdoor room posed a serious problem. A 7.0 ton (rated capacity) NESLAB HX-750 chiller uses ethylene glycol as the secondary fluid removes heat from the outdoor room through a coil and blower system. The heat transfer on the coil is:

(1) $$Q_{coil} = UA * LMTD$$

where LMTD is the log mean temperature difference, and UA is the overall heat transfer coefficient for the coil.

The overall heat transfer resistance in the coil includes both air-side and refrigerant-side heat transfer resistances (neglecting the heat transfer resistance of the metal) as follows:

(2) $$\frac{1}{UA} = \frac{1}{h_{air}\left(A_p + \eta A_e\right)} + \frac{1}{h_{ref}A_{ref}}$$

where A_p is the air-side prime area (the outside area of the tubes), A_e is the air-side extended area (the area of the fins), n is the fin efficiency, A_{ref} is the refrigerant-side area (the internal area of the pipes), h_{air} and h_{ref} are the air and refrigerant-side convective heat transfer coefficient respectively.

Stoecker and Jones (1982) roughly estimated the convective heat transfer coefficient for the air side as:

(3) $h_{air} = 38\sqrt{V}$

where V is the air face velocity in meters per second.

The UA value for the coil and the refrigerant-side convective heat transfer coefficient were calculated using the coil manufacturer's data for two runs at dry conditions. The UA and effectiveness were also calculated from temperatures measured in a very crude manner at those conditions, and the results were closest to the manufacturer's data for the second data point. These approximate results provided the basis for estimating the extent to which outdoor room performance might be further improved.

Tairin	Tairout	Trservoir	Treturn	UA [Btu/h-F]	effectiveness
75	53	40	44	1749	0.62
90	61	40	46	1546	0.59

Table C.2.3: Outdoor room coil manufacturer's data.

As expected, the air side accounted for most of the heat transfer resistance at 71%. Therefore, a bigger benefit would come from reducing the resistance on the air side than on the refrigerant-side. There are two options for improving the air-side resistance, increase the area (use a bigger coil), or increase the convective heat transfer coefficient (use a bigger blower). The coil fits perfectly in the air duct, therefore replacing the blower was considered the better option in case it becomes necessary to improve the heat transfer in the coil. Obviously, adding another coil downwind of the existing one, would also increase the UA.

C.3 Chiller Re-piping

The chiller pump was operating close to the maximum pressure drop prescribed by the manufacturer. Therefore, the chiller piping was modified to decrease the pressure drop in the chiller, and increase the ethylene glycol mass flow rate. With the modified chiller piping, the glycol flow rate increased from 14 to 18.5 gallons per minute. This 32% increase in flow rate yielded only a 6% increase in UA because the glycol-side heat transfer coefficient increased as Reynolds number to the 0.8 power, but affected only 29% of the overall resistance. An equivalent increase in the air flow would provide a 10% in UA, assuming that the air-side heat transfer coefficient varies with velocity to the 0.5 power. This would lead to the conclusion that increasing the air flow would be much

53

more attractive, however increasing the ethylene glycol flow was much more easily accomplished, and it is also expected to increase the pump operating life.

Another way to express the heat transfer in the coil is:

$$(4) \qquad Q_{coil} = \varepsilon \times \left(w C_p \right)_{min} \times \Delta T_{max},$$

where ε is the coil effectiveness, $(wC_p)_{min}$ is the minimum mass flow times specific heat for the two fluids (in this case air), and ΔT_{max} is the maximum temperature difference between the two fluids. The coil effectiveness was determined using the coil data. The air mass flow through the coil can be assumed to be a constant rated at 1500 SCFM by the manufacturer. The maximum temperature difference is equal to the air inlet temperature (the outdoor room temperature) minus the glycol inlet temperature (the glycol reservoir temperature assuming the heat transfer loss in the supply line is negligible).

From the two dry-coil data points examined, it became clear that the coil is undersized. Its effectiveness is only around 55-60% at the maximum air and glycol flow rates.

The chiller cooling capacity depends on the fluid temperature, ambient temperature, and cooling fluid (NESLAB, 1991). The chiller cooling capacity for a chiller operating at 68°F ambient temperature, with water as the cooling fluid (specific heat of 1 Btu/lb$_m$-°F) is shown in Figure C.3.1 for a varying ethylene glycol temperature.
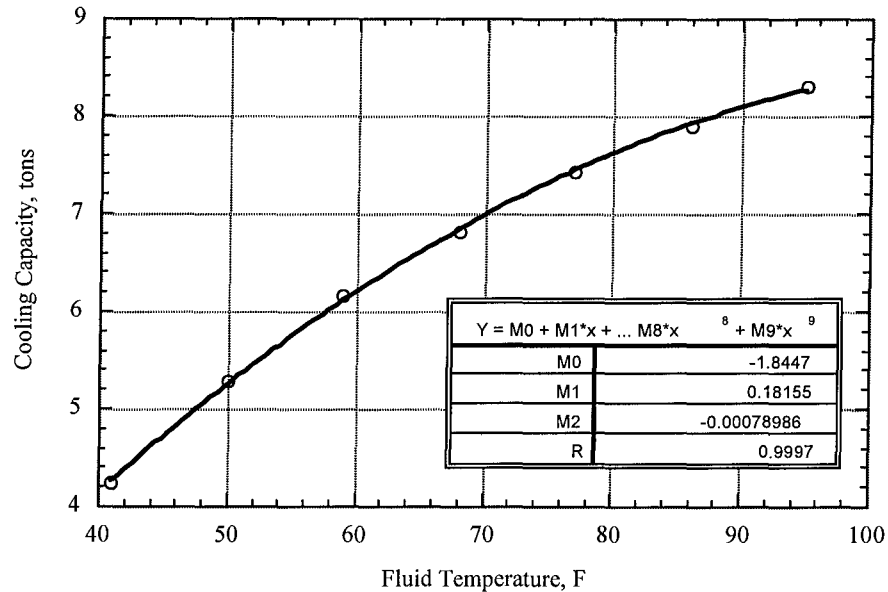
Figure C.3.1: Chiller cooling capacity.

The embedded equation and table in the figure:

$$Y = M0 + M1 \cdot x + \dots M8 \cdot x^8 + M9 \cdot x^9$$

M0	-1.8447
M1	0.18155
M2	-0.00078986
R	0.9997

Axis labels: Cooling Capacity, tons (y-axis); Fluid Temperature, F (x-axis)

A curve fit of the cooling capacity versus fluid temperature for the chiller provided an equation for the maximum chiller heat transfer as a function of the ethylene glycol temperature.

C.4 Test Matrix

This model was then used to check which test conditions the facility would be able to maintain with the new unit. The test matrix includes 13 dry data points and 5 wet data points and it is shown in the Table C.4.1. A simulation model was used to determine the condenser loads for the 2.5 ton split system, and the EES model was used to predict the outdoor room coil capacity for the test matrix conditions.

Data Point	Tindoor DB/WB (°F)	Toutdoor DB/WB (°F)	Qcond (Btu/hr)	WRR (lbm/hr)	Max. Qcoil (Btu/hr)
1	81/67	83/59	34097	0	44239
2	68/48	67/48	30171	0	34970
3	68/50	95/60	29632	0	50946
4	68/52	115/67	29342	0	61576
5	81/56	73/53	34433	0	37320
6	81/58	95/62	33802	0	50946
7	81/59	115/69	33359	0	61576
8	96/62	76/54	39441	0	40227
9	96/62	96/62	38717	0	51495
10	96/63	116/69	38095	0	62087
11	116/69	86/57	46006	0	45937
12	117/69	96/61	45849	0	51495

13	116/55	111/67	44750	0	59511
14	81/67	96/84	36108	6.03	51495
15	81/63	96/80	34015	0.61	51495
16	101/75	96/82	40792	0.75	51495
17	101/78	96/83	42384	4.69	51495
18	101/84	96/86	46386	14.5	51495

Table C.4.1: Test matrix and outdoor room capacity.

Table C.4.1 shows that the chiller should be able to easily handle the outdoor room load for most operating conditions. The calculated outdoor room load and coil capacity for data points 8 and 11 are virtually the same, and it would be difficult to predict whether or not the facility can handle those points. These data points are extreme cases that have a considerably higher indoor than outdoor temperature. The most problematic points combine high condenser heat rejection into a cool outdoor room, and low glycol temperatures that hinder the chiller cooling capacity. High condenser heat rejection can be cause by either sensible or latent loads in the indoor room.

C.4 Outdoor room temperature control

It is difficult to anticipate the exact glycol supply temperature needed to achieve a given outdoor room temperature setpoint. This is achieved by controlling a bypass valve that reduces the glycol flow rate. The range of this control is determined by two extreme cases: sending the full 18 gpm through the coil, or sending only the amount required to remove the condenser heat load shown in the Table above. Since the heat capacity of glycol is about 7500 Btu/°F, its return temperature is generally only 4-6°F greater than its supply temperature. On the other hand, the (dry) air stream's heat capacity is about 1700 Btu/°F, so its temperature changes by about 20-30°F.

Two conclusions are obvious. First, a larger coil would enable the chiller to supply glycol at warmer temperatures: perhaps only 30°F cooler than the outdoor room. This would enable the chiller capacity to exceed the test unit's condenser load by margins greater than those seen in Table C.4.1. The second observation is that large changes in the glycol flow rate can have only limited effect on capacity. Even changing to water, with its higher specific heat and higher heat transfer coefficients, would have only a small impact.

For the loads shown in the Table, about 30-50,000 Btu/h, the LMTD's range from 20-30°F, given the approximate UA determined from the dry-coil tests. Therefore halving the glycol flow rate while holding its supply temperature constant would increase the glycol return temperature by an additional 4-6°F, having only a small effect on the LMTD and capacity.

Figure C.4.1 shows the effect of reducing glycol flow rate enough to raise its return temperature from a 45°F supply temperature all the way to the air inlet temperature; that is, the outdoor room temperature. Calculations were done assuming that only 80% of the manufacturer's rated chiller capacity can be realized at the coil in the outdoor room, due to line losses, lower return temperatures, and the use of a 50% glycol mixture instead of water. The effect of full chiller capacity (f_chiller = 1) is also shown for one condition. Actually the glycol turndown ratio need not be as large is shown here, because the coil UA will not remain at its maximum value as assumed; it will decline as glycol mass flow rate decreases from its maximum 18 gpm.

Fortunately the condenser heat rejected by the air conditioner is insensitive to outdoor room temperature, as shown in Table C.4.1. It changes by only a few thousand Btu/h as outdoor room temperature is allowed to rise from its minimum value to the top of the test matrix at about 120°F. This occurs because refrigerant mass flow rate and therefore system capacity decreases as the compressor pumps against a higher discharge pressure. Fortunately the increased compressor power is offset almost exactly by the decline in heater and humidifier power needed to maintain constant conditions in the indoor room.

57
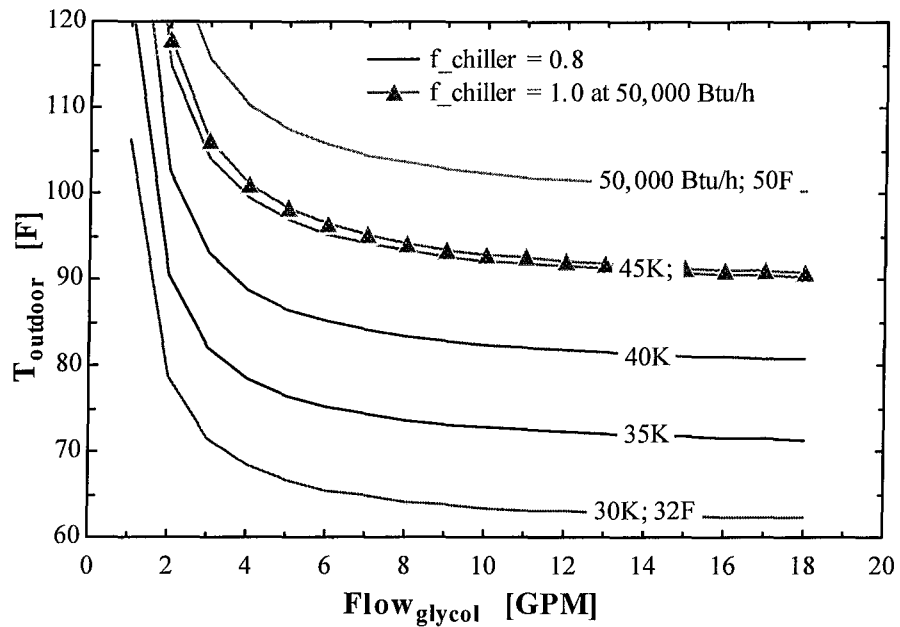
Figure C.4.1: Outdoor room temperature versus glycol temperature and volumetric flow.

Figure C.4.3 shows the effect of using a bypass valve to reduce the flow of glycol through the coil. Since the heat load remains nearly constant, the lines on the graph show the range over which outdoor room temperature can be controlled. The maximum glycol supply temperature is also shown on the graph, assuming that 80% of the chiller's rated capacity is realized at the outdoor room coil. Since the chiller capacity is more than adequate at the higher supply temperatures, it would be possible to operate the chiller at a lower supply temperature. However this would require greater reductions in glycol flow rate through the coil. Therefore the higher glycol temperatures would be acceptable, unless lower temperatures in the outdoor room were required. The magnitudes of the horizontal asymptotes reflect two effects: chiller capacity and coil effectiveness. Figure C.4.3 suggests that the best control strategy is to close the bypass valve, and then set the glycol supply temperature at the level that provides the lowest outdoor room temperature. Then the higher temperatures can be achieved by opening the bypass control valve.

58
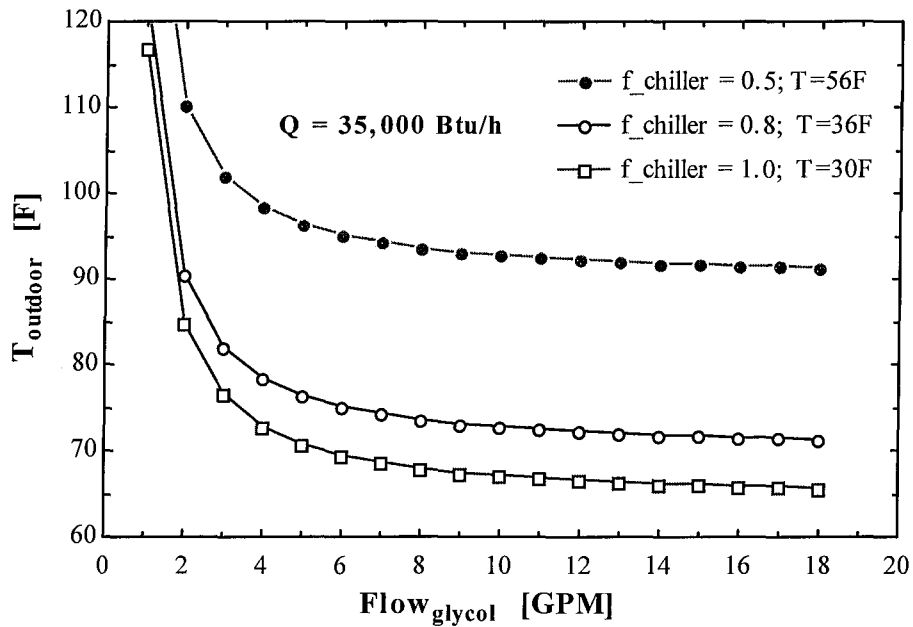
Figure C.4.2: Effect of control valve on outdoor temperature for different bypass valve settings.

It is clear from Figure C.4.1 that the glycol supply temperature must exceed 0°C in order for 80% of chiller capacity to be sufficient for even the lowest loads expected in the test matrix. Figure C.4.3 shows that the outdoor room temperature cannot be pulled down below 60°F, unless the glycol coil is replaced by one having a larger UA. It is also clear that the difference between 80% and 100% chiller capacity is significant.

The figures also show that the glycol pump has plenty of capacity; the problem is to reduce the flow through the coil enough to allow room temperatures to rise. This requires shutting the inline valve at the glycol entrance to the coil. Without it, the coil pressure drop is of the same order of magnitude as the control valve pressure drop, so the flow through the coil is relatively insensitive to the control valve position. Figure C.4.3 shows results of calculations showing the minimum coil flow rates achievable when the inline valve is set to 4 different positions with the bypass control valve wide open.

2.0 ⎯⎯⎯⎯⎯⎯⎯⎯⎯⎯⎯ 50.00

1.8 ⎯⎯⎯⎯ 45.00

1.5 ⎯⎯⎯⎯ 40.00

1.2 ⎯⎯⎯⎯ 35.00

dP_{coil} [psi]   1.2 ⎯⎯⎯⎯ 30.00 $dP_{coil,max}$ [psi]

1.0 ⎯⎯⎯⎯ 25.00

0.8 ⎯⎯⎯⎯ 20.00

Calculations assume total flow = 17 gpm   15.00

0.5 ⎯⎯⎯⎯ 10.00

⎯o⎯ Actual dP across cv and coil+inline valve

0.2 ⎯⎯⎯⎯ 5.00

⎯●⎯ dP across coil and inline valve when cv shut

0.0 ⎯⎯⎯⎯ 0.00

0   1   2   3   4   5   6

Flow$_{coil}$ [gpm]
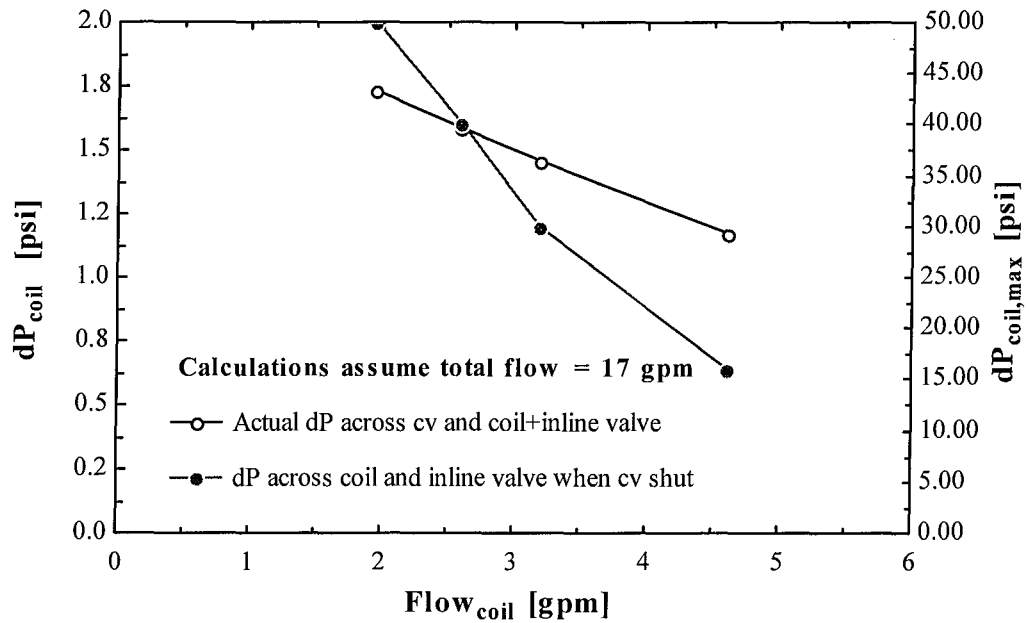
Figure C.4.3: Pressure drop versus volumetric flow.

Note that the actual pressure drop at these conditions is less than 2psi across the control valve and the coil plus its inline valve. The right hand scale and the solid dots show the pressure drops observed across the coil and inline valve with the bypass valve shut. These readings were taken to determine the flow coefficient for the inline valve in 4 discrete positions, ranging from about 50-70% shut.

Finally Figure C.4.3 is based on the assumption that total flow of glycol from the chiller pump equals 17 gpm. Other calculations and experimental observations demonstrated that the pump flow rate is insensitive to the small changes in pressure drop across the coil, inline valve and control valve. It does, however, drop to about 10 gpm when the bypass control valve is shut and the inline valve is experiencing its maximum 50 psi pressure drop.

C.5 Chiller Troubleshooting (By Derek Harshbarger. October 1998)

This appendix describes the troubleshooting of the Neslab instruments HX-750 recirculating chiller. R-22 is the active fluid in the system, despite the mention of R-500 in the original purchase order. There should be 20 lbm of charge in the system. The particular model that is in use is a special low temperature version which uses two thermal expansion valves (TXV's). Also worth noting is that the Neslab engineering

60

technical service persons are the only department contacted that had knowledge about the special low temperature model.

The TXV that is closer to the Glycol bath has a 5 ton capacity and the TXV that is away from the glycol bath has a 2 ton capacity. These TXV's can operate either in tandem or individually. Two control dials dictate the combination of TXV's that is necessary at a given temperature. These dials are located on the back wall of the chiller. The dial closer to the outermost wall of the chiller is used to determine when the system will change from using both TXV valves and using one TXV. The dial closer to the glycol bath controls at what temperature the 5 ton TXV will switch off and the 2 ton TXV will activate. According to Neslab, the dials should be set at 65°F and 32°F respectively.

The TXV's should be set at 18°F superheat. In order to correctly measure the superheat , the temperatures must be measured at the evaporator inlet and the suction line. Specifically, the suction line temperature must be taken where the TXV bulbs are attached, downstream of the evaporator exit. If it were measured closer to the evaporator exit, the TXV bulb might be splashed by liquid droplets that may still exist in the superheated stream. The suction like is probably insulated to prevent loss of compressor capacity.

On the condenser, there are two blowers. When looking at the back of the chiller, the left blower should be running anytime the chiller is on. The right blower is controlled by pressure transducers in the system. During our testing, it was observed that the right blower never activated when increased capacity was desired. As a technician's fix to run the second blower continuously, the leads were switched at the control box. The control box is located on the back of the chiller, below the glycol bath. Inside the box there is a cylinder that has slots for three sets of two leads. The set closest to the back of the system was originally unused. Following the technicians advice, the leads were switched from the second to the third spots. This forces the second blower to remain on continuously.
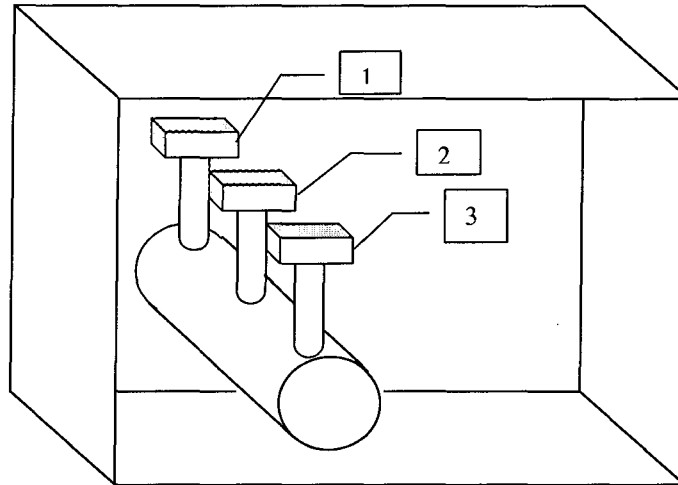
Figure C.5.1: Blower Control Box.

During the troubleshooting with the Neslab technicians, the suction line and discharge line pressures were measured. The suction line was measured at the accumulator with a Schrader valve port. The discharge line was measured with the a rotolock port. This port requires a pressure gauge to be attached. Then removing the black plastic cap and turning the long square cross-sectioned step one complete revolution clockwise. This stem should be as long as possible when it is closed. The reverse process should be used to disconnect the pressure gauge. The pressures should be around 80 – 90 psig and 225 psig for the suction and discharge pressures respectively.

During normal operation, the system should oscillate between cooling and idle modes. Lights on the control panel indicate which mode is in operation. During the no load tests, it was observed that the glycol bath temperature never dropped below 0°C. The indicator did read negative zero, but as soon as the 2 ton TXV turned on (while the 5 ton turned off) the glycol bath temperature increased to 2°C. When the glycol reaches 2°C the TXV's switch to cool the bath to the negative zero indicator reading.

Appendix D

Capillary Tube Dimensional Study

D.1 Introduction

The function of the capillary tube is to provide for isenthalpic expansion of the refrigerant flow. Two modes of energy dissipation occur in the capillary tube, pressure drop due to friction in the capillary tube, and pressure drop due to the shock wave at the entrance to the evaporator. This shock wave may produce unwanted noise in the a/c unit, therefore, one of the objectives when designing a capillary tube may be to obtain a lower outlet pressure to minimize the shock wave. The resulting higher exit velocity and quality in the downstream section of the tube may produce an unwanted hissing noise. Until more is known about the tradeoffs between these two sources of noise, an optimum cannot be defined. Therefore this analysis defines the parameter space within which these tradeoffs can be analyzed.

For a given flow condition at the condenser exit (refrigerant pressure and degree of subcooling), the mass flow through the capillary tube depends on the physical dimensions of the capillary tube, and the number of capillary tubes in parallel.

This Appendix presents simulation results for a 1.5 ton Whirlpool room a/c unit having 287 psi pressure, and 10.0°F subcooling at the exit of the condenser at a design condition of 80°F indoors, and 95°F outdoors.

D.2 Number -- Diameter -- Length (NDL) Trade-offs

Figure D.2.1 shows several diameter and length combinations that provide the same mass flow under a fixed inlet condition (inlet pressure and degree of subcooling) for 1 to 5 capillary tubes in parallel as determined by a computer simulation model. These capillary tube dimensions found in this simulations will be used throughout this Appendix to study capillary tubes.
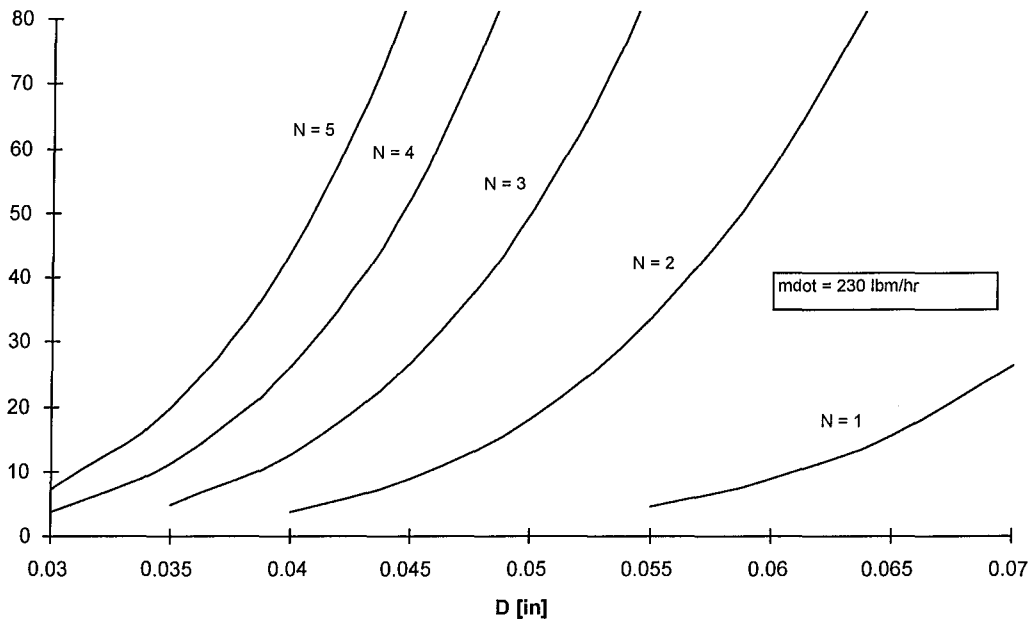
Figure D.2.1: Capillary tube NDL combinations that provide the same mass flow.

Figure D.2.1 shows that a higher number of capillary tubes that are longer and with the same diameter, or thinner and with the same length can replace a given number of capillary tubes. The number of tubes is often dictated by the circuiting of the evaporator and the need to distribute flow evenly among the parallel circuits. For a fixed number of capillary tubes, the thicker the capillary tube, the longer it has to be.

D.3 Robustness

Figure D.3.1 shows a computer simulation of how system EER of the Whirlpool test unit responds to off-design conditions of a wide range of ambient temperatures (the indoor temperature was kept at 80 °F). It shows that the NDL combination chosen by the designer has a negligible effect on EER under a wide range of conditions.
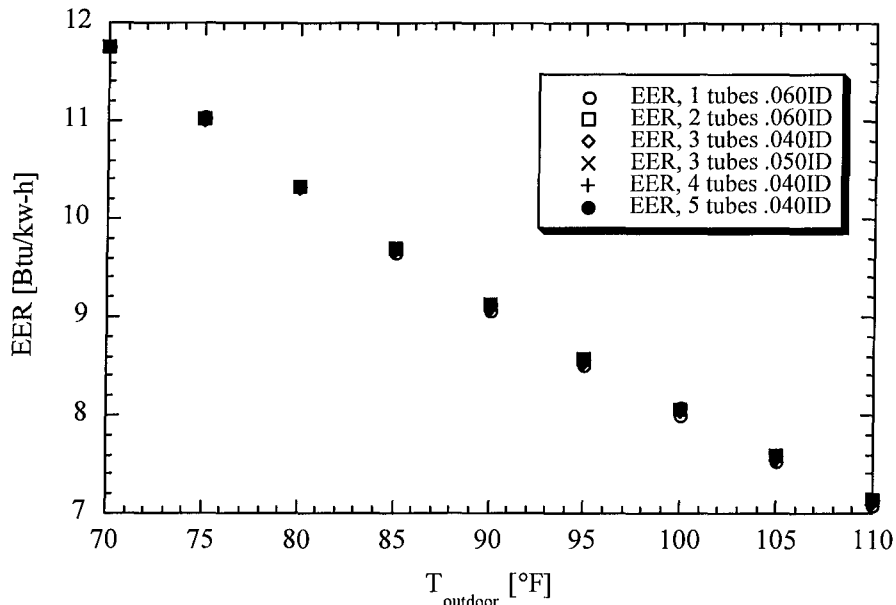
Figure D.3.1: Effect of ambient temperature on EER for several capillary tube NDL combinations.

Therefore the cooling system designer can choose among an infinite number of capillary tube combinations that will provide the same mass flow, and keep the same system performance. Outlet conditions is these simulations, however, differed significantly among the different capillary tube combinations. Figure D.3.2 shows the capillary tube critical pressure varies with different capillary tube NDL combinations.

Since the flow at the exit is usually choked, the critical pressure is independent of the evaporator pressure. However the absolute pressure at the exit is determined by the NDL combination as well as the condensing pressure. It is important to know the conditions under which the exit pressure may approach the evaporator pressure. The absolute value of the exit pressure has an important effect on the possibility of clogging and the noise produced in the tube, as discussed bellow.

Figure D.3.2 also shows that the relationship between capillary tube geometry and outlet pressure is maintained throughout the range of normal ambient conditions. The difference in outlet pressure between two different capillary tube NDL combinations is independent of ambient temperature. Therefore, it appears that one can concentrate on

studying capillary tube trade offs at one design condition, and extrapolate those results for other conditions.
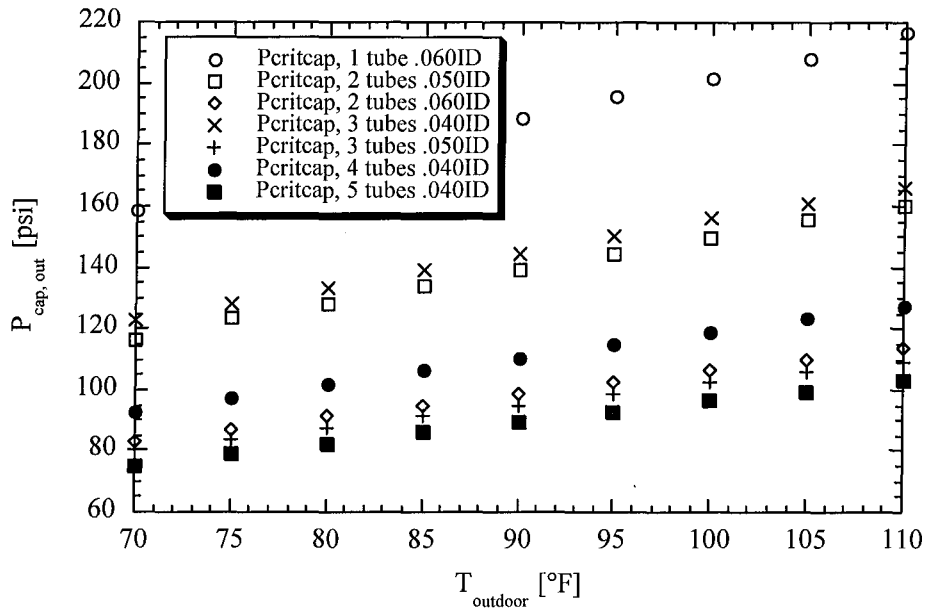

Figure D.3.2: Capillary tube exit pressure for several capillary tube NDL combinations versus ambient temperature.

D.4 Effects of Exit Conditions

Friction against the tube wall is the main cause of pressure drop inside tube. Therefore, pressure drop inside the tube is largely a function of the capillary tubes internal area. Figure D.4.1 shows the relationship between tube area and critical exit pressure. A larger tube internal area provides more pressure drop inside the tube, and therefore a lower critical pressure. In other words, for a given mass flow rate and number of tubes, a thicker and longer capillary tube will dissipate more energy via pressure drop inside the tube than a thinner, shorter tube.
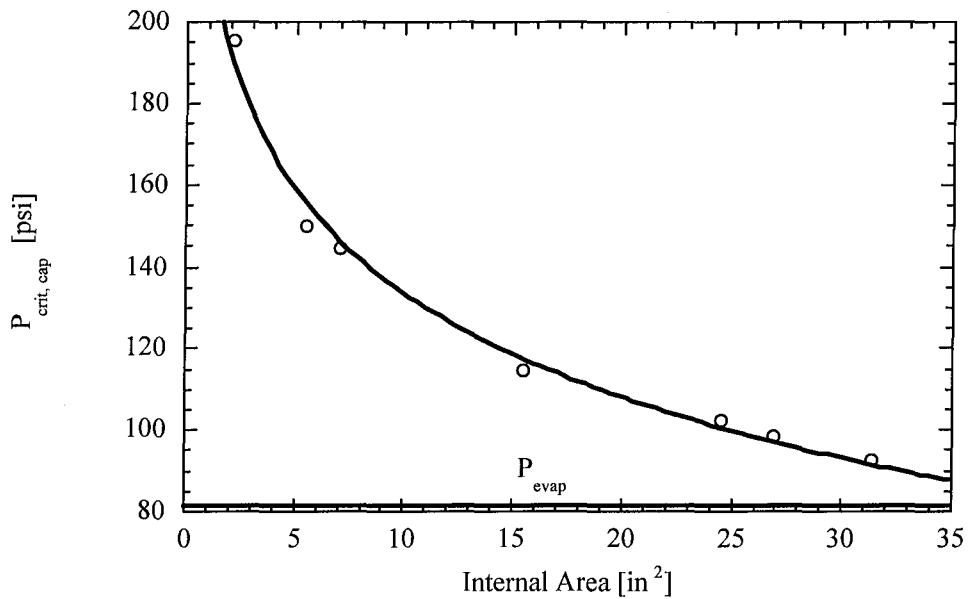
Figure D.4.1: Capillary tube outlet pressure versus tube surface area at 80-95 conditions.

Figure D.4.2 shows how outlet pressure increases as the number of capillary tubes running in parallel decreases. This would increase the strength of the shock wave at the evaporator entrance, and therefore the shock-related noise. For a fixed number of capillary tubes, thicker and longer tubes produce lower outlet pressures. Therefore many, thick, long capillary tubes achieve lower outlet pressures, that might even equal the evaporator pressure, eliminating the shock wave at the evaporator entrance.
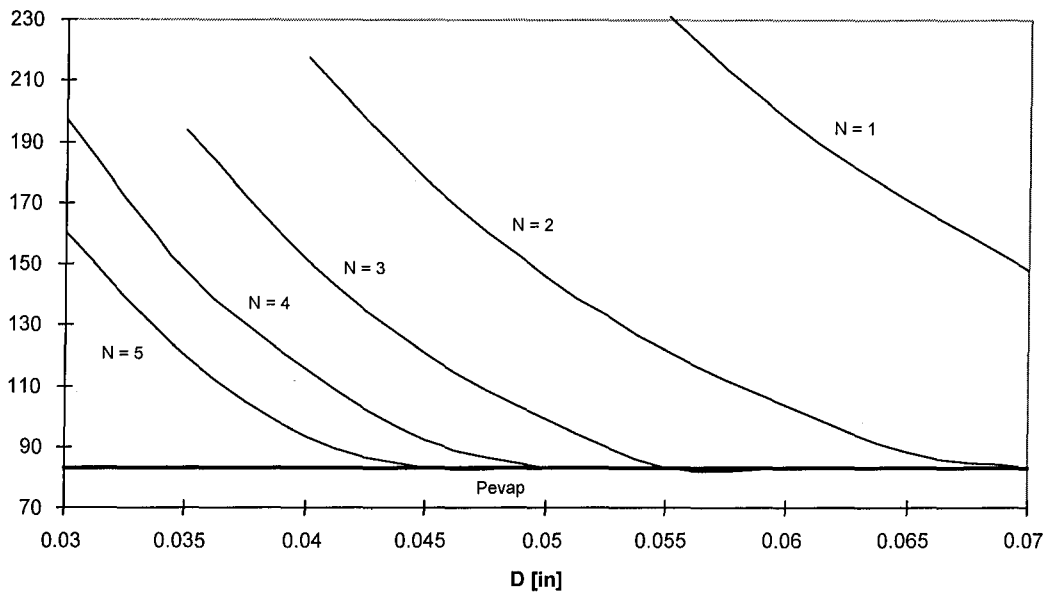
Figure D.4.2: Capillary tube outlet pressure versus diameter for 1 to 5 capillary tubes in parallel.

Figure D.4.3 indicates that for a given mass flow and inlet conditions, the ratio of capillary tube length over diameter is the key parameter that determines the outlet pressure, independent of the number of capillary tubes. Therefore the designer could choose the length/diameter ratio such that the capillary tube exit has the desired critical pressure based on noise, clogging potential and other considerations.
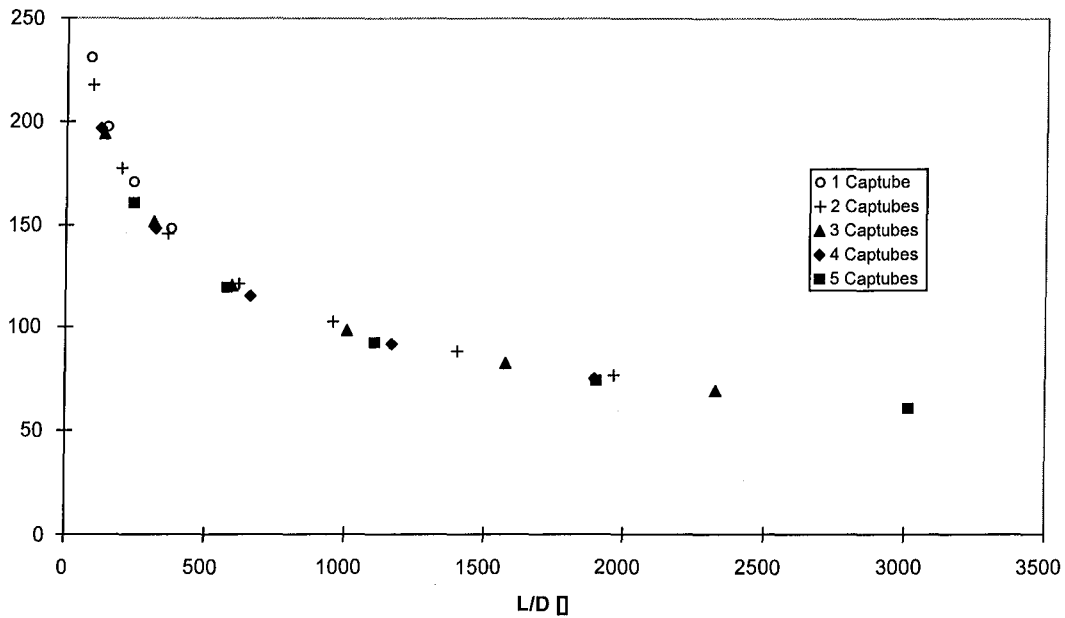
Figure D.4.3: Capillary tube outlet pressure versus length over diameter ratio for 1 to 5 capillary tubes.

Another concern when designing capillary tubes is clogging. Clogging occurs in two different modes: oxidation at the entrance, and oil deposition at the exit. As the refrigerant temperature drops, oil viscosity increases, and the oil tends to get stuck at the tube walls. Therefore, tubes that provide a higher critical pressures have a lower tendency to clogging than tubes with low critical pressures. Another factor that influences clogging at the capillary tube exit is the refrigerant velocity. High velocities are likely to thin the oil layer on the tube walls. Figure D.4.4 shows how the refrigerant critical pressure and velocity varies with internal area. Capillary tubes with higher internal area have higher critical velocities at the tube outlet, which keeps the oil moving fast, but on the other hand, have the lowest outlet temperature and therefore the lower oil viscosity.

69
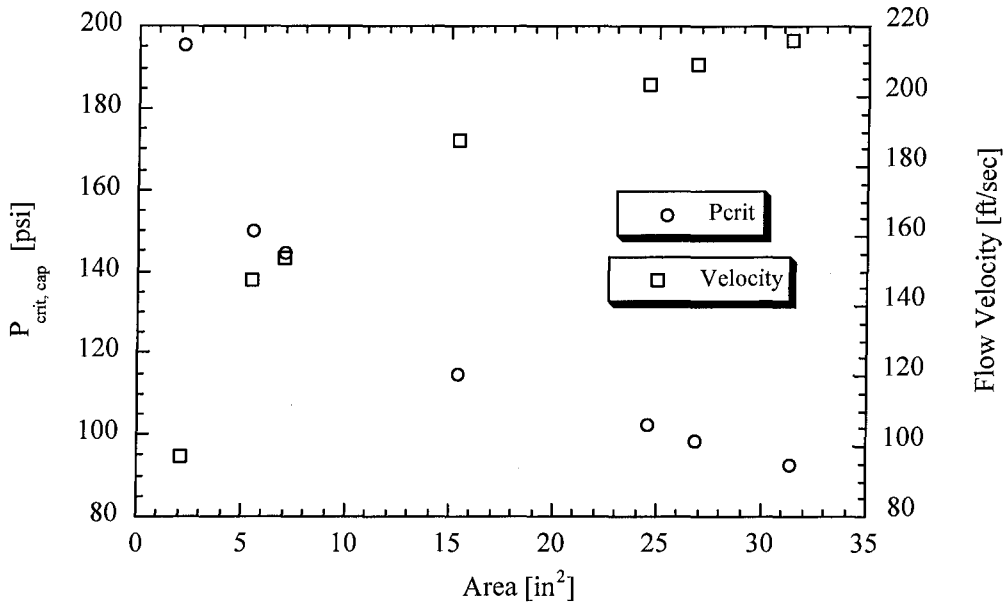
Figure D.4.4: Capillary tube outlet pressure and velocity for several NDL combinations versus internal area.

D.5 Capillary tube model changes

Before conducting this capillary tube dimensional study, some improvements were made to the capillary tube model.

D.5.1 Sub-sonic exit case

On most operating conditions, the critical pressure at the exit plane of the capillary tube is higher than the evaporator pressure. The model takes advantage of this fact, and assumes a choked exit for its calculations. Assuming that the critical pressure and exit quality are known, the model can calculate the critical mass flux, and then backtrack to the capillary tube entrance. Then it checks the calculate entrance conditions and capillary tube length against the actual values. Then the model makes a new assumption for the exit pressure and quality, and iterates until the entrance conditions are satisfied.

However, in some cases, for example during initial start-up, the evaporator pressure may be higher than the critical pressure, so the capillary tube will have a sub-

sonic exit. The model was modified to account for such a case. In such cases, the exit pressure is equal to the evaporator pressure, and the model assumes values for the mass flux and exit quality. Then it backtracks to the entrance, compare the calculated entrance conditions with the actual conditions, and adjusts the assumed values for mass flux and exit quality.

D.5.2 Metastable correction

Theoretically, the refrigerant flash point in the capillary tube occurs when the refrigerant pressure is equal to the saturation pressure corresponding to the refrigerant temperature. However, a finite amount of superheat is required for the formation of the first vapor bubble. Therefore, a metastable liquid region exists at pressures below saturation pressure. The effect of this metastable region is that the actual capillary tube flow rate will be greater than the flow rate that would exist under ideal thermodynamic equilibrium conditions (Yin, 1998). A metastable correction initially developed by Chen et al. (1990) and later modified based on experimental data by Yin (1998) was incorporated to the model.

References

ANSI/ASHRAE Standard 62-1989, "Ventilation for Acceptable Indoor Air Quality." *ASHRAE*, 1989.

American Society of Heating, Refrigeration and Air-conditioning Engineers, "Handbook of Fundamentals." *ASHRAE*, 1997.

Bridges, B.D. and C.W. Bullard, "Simulation of Room Air Conditioner Performance." *University of Illinois at Urbana-Champaign*, ACRC-TR-79, 1995.

Carrier Corporation, 1996, *Air Conditioner Product Data from 38TXA-IPD, Catalog No. 523-846*, Syracuse, NY, pp 16.

Chen, Z.H., R.Y. Li, S. Lin, and A.Y. Chen, "A Correlation for Metastable Flow of R-12 Through Capillary Tubes," *ASHRAE Transactions,* 96(1) pp. 550-554, 1990.

Chuah, Y.K., C.C. Hung and P.C. Tseng, "Experiments on the Dehumidification Performance of a Finned Tube Heat Exchanger." *HVAC&R Research*, vol. 4, no. 2, pp. 167-178, April 1998.

Elmahdy A.H. and R.C. Biggs, "Finned Tube Heat Exchanger: Correlation of Dry Surface Heat Transfer Data." *ASHRAE Transactions*, vol. 85, no. 2, pp. 262-273, 1979.

Gray, D.L. and R.L. Webb, "Heat Transfer and Friction Correlations for Plate Finned-Tube Heat Exchangers Having Plain Fins." *Proceedings of the 8th International Heat Transfer Conference*, vol. 6, pp. 2745-2750, 1986.

Harriman III, L.G., D. Plager and D. Kosar, "Dehumidification and Cooling Loads From Ventilation Air." *ASHRAE Journal*, pp. 37-45, November 1997.

Kirby, E.S., C.W. Bullard, and W.E. Dunn, "Effect of Airflow Nonuniformity on Evaporator Performance," *ASHRAE Transactions*, 104:2, 755-762, 1998.

Kosar, D.R., M.J. Witte, D.B. Shirey III and R.L. Hedrick, "Dehumidification Issues of Standard 62-1989." *ASHRAE Journal*, pp. 71-75, March 1998.

Krakow, K.I., S. Lin and Z.S. Zeng, "Temperature and Humidity Control During Cooling and Dehumidifying by Compressor and Evaporator Blower Speed Variation." *ASHRAE Transactions*, vol. 101, no. 1, pp. 292-304, 1995.

Nakayama, W. and L.P. Xu, "Enhanced Fins for Air-cooled Heat Exchangers - Heat Transfer and Friction Correlations." *ASME-JSME Thermal Engineering Joint Conference Proceedings*, vol. 1, pp.495-502, 1983

NESLAB Instruments Inc., "HX Recirculating Series." 1991.

Porter, K. P., personal communication, University of Illinois Air Conditioning & Refrigeration Center, Urbana, 1996.

Stoecker, W.F. and J.W. Jones, *Refrigeration and Air-conditioning*, 2nd Ed., New York: McGraw-Hill, 1982.

Wang, C.C. and Chang, C.T., "Heat and Mass Transfer for Plate Fin-and-Tube Heat Exchangers With and Without Hydrophilic Coating." *International Journal of Heat and Mass Transfer*, vol. 41, no. 20, pp. 3109-3120, 1998.

Yin, J. M., *Private Communication*, University of Illinois Air Conditioning & Refrigeration Center, 1998.

Yin, J. M., "A theoretical model for predicting adiabatic capillary tube performance: an analysis and improvement." *ACRC TR-139, University of Illinois Air Conditioning & Refrigeration Center*, 1998.